Chapter 3

Intermittency and related issues

3.1 Introduction

The investigation of single particle density fluctuations in narrow phase space intervals has been a popular method to study the mechanism of multiparticle production [1–5]. Most of the analyses in this regard are based on the measurement of scaled factorial moment (SFM), that can eliminate Poisson distributed statistical noise. Bialas and Peschanski [6, 7] first pointed out that the single particle density functions should be examined locally within narrow intervals and not over the entire region of phase space accessible to an experiment. They employed the SFM-technique to analyze the JACEE events induced by ultra-relativistic cosmic ray nuclei [8], and found that the q-th order SFM (F_q) for integer q, increases with decreasing phase space resolution size δX as,

$$F_q \propto (\delta X)^{-\phi_q} \qquad \text{as} \;\; \delta X \to 0 \tag{3.1}$$

In high-energy physics the phenomenon is known as 'intermittency'. A scale invariant exponent ϕ_q extracted from the phase space dependence of F_q, represents the intermittency strength and characterizes the dynamical part of the density fluctuations. Several speculative suggestions have so far been made to interpret the origin of dynamical components in particle density fluctuation. The most common trivial reasons of fluctuation are the statistical noise, kinematic conservation laws, quantum correlations etc. The dynamical

fluctuations on the other hand may arise due to (i) collective flow (ii) formation of mini-jets, (iii) emission of Cerenkov gluons [9] (iv) a random cascading effect in the space-time evolution of the collision process [10], (v) a parton-hadron phase transition [11], and (vi) a combination of more than one or all of the above [9, 12–15].

In order to better understand the characteristics of local density fluctuations, an intermittency analysis is usually supplemented by the factorial correlator (FC), oscillatory moment (OM) and erraticity moment analysis. While the SFM accounts for local fluctuations about a particular phase space point, the correlation among particles at different phase space points, located at a distance larger than the scale size at which the correlations are being examined and generated by the intermittency type of fluctuations, are usually characterized by the two-fold factorial correlator (FC) [6, 7]. Both the SFM and the FC are actually integrals of the same underlying correlation function, but they differ only with respect to the respective domains of analysis. This close relationship between the two can be traced back into the sum rules involving the SFM and the FC. Both moments are sensitive to the projection (dimensional reduction) effects and both contain contributions from the corresponding lower-order moments. The OM on the other hand, provides a deeper insight to the multiparticle dynamics [16, 17], e.g., the gluon-dynamical equation predicts a minimum in the OM at a rank $q \approx 5$. One should however keep in mind that the OM is effective only to the partonic multiparticle dynamics [17]. The nature of event-by-event fluctuations beyond intermittency is investigated by using the erraticity moments [18–20], which are free from some of the disadvantages of the SFMs. One such limitation is that the SFMs are incapable of locating the position of a spike or a sharp void in an event. Moreover, while averaging over a large event sample, the characteristic event space fluctuations of the SFMs are smoothed out. Two important pieces information can be extracted from an erraticity analysis. First, it quantifies the chaotic nature of spatial fluctuations in the event space, and second, it is capable of characterizing the degree of fluctuation of the parton multiplicity that initiates the QCD branching processes. It is claimed that in order to describe the chaoticity of multiparticle production in high-energy interactions, the entropy index (μ_q) is as effective as the *Lyapunov exponent* is for describing a classical deterministic nonlinear system [19, 20]. Non-vanishing positive values of μ_q can be used as a criterion for the purpose. In this chapter we present some results on the intermittency and related issues for the ^{16}O-Ag/Br interaction at an incident momentum of 200A GeV/c. The results are sometimes compared with the results obtained by using a set of ^{32}S-Ag/Br data at 200A GeV/c presented in a previous analysis [21]. We also systematically compare the experimental results with those obtained from the UrQMD and UrQMD+BEC simulations.

3.2 Literature review

As mentioned above the analysis of local density fluctuations of particles within narrow intervals of phase space in terms the SFM was for the first time suggested by Bialas and Peschanski [6] for the cosmic-ray induced AgBr events recorded by the JACEE collaboration [8]. It was found that the SFM in general increases with decreasing rapidity resolution (δy) following a scale invariant power law. The word intermittency was coined from the turbulence in hydrodynamics. The intermittency phenomenon proves that the particle density fluctuations must have some dynamical origin [18–20, 22, 23]. Holynski *et al.* [24] studied the SFM in proton-emulsion interactions at 200 and 800 GeV, and in ^{16}O-emulsion interactions at 60A and 200A GeV. Clear evidence of short-range dynamical correlations was observed from the data that could not be explained by Monte Carlo (MC) simulations. Standard models of multiparticle production could not explain the intermittent behavior either [25]. On the other hand, a jet model that used a scale-invariant decay function, appeared to be consistent with the intermittency results. From the 1d and 2d SFM analysis in p-nucleus, ^{16}O-AgBr and ^{32}S-Ag/Br interactions at 200A GeV (EMU07 experiments), it was found that the intermittency phenomenon is much stronger in the (η, φ)-space than in the η-space [26]. The intermittent pattern was more pronounced in the p-nucleus interaction than in the AB interactions. The results of intermittency analysis in ^{32}S+Au interaction at 200A GeV (EMU01 collaboration) were compared with the results simulated by the Lund Monte-Carlo model, FRITIOF [27]. The FRITIOF results showed a bin size dependence only for a horizontal averaging scheme of the SFM, but was found to be uniform with $\delta\eta$ for the vertical averaging. Using the ^{16}O-emulsion and ^{32}S-emulsion data at 60A and 200A GeV (EMU08 Expt.) [28–30], and p-emulsion data at 800 GeV (FNAL Expt. No. 751) [31, 32], it was shown that at a given incident energy the 1d intermittency strength decreases with increasing event multiplicity. However, the same strength slowly increases with the mass number of the projectile nucleus. In nuclear emulsion experiments held at a few GeV/nucleon energy range, presence of intermittency was found in the η and φ-distributions of the shower tracks [33]. However, the generalized dimensions (D_q) computed from the intermittency index did not depend either on the reaction type or on the energy of the collision [32–35]. In another study of the p-nucleus interaction at 800 GeV [36], the intermittency index was found to corroborate the above observation on D_q. An energy dependence of the intermittency exponent obtained from the ^{16}O+Ag/Br interaction at 60A and 200A GeV was reported [37]. In a comprehensive study on the intermittency and cumulant moments using the ^{28}Si-emulsion and ^{197}Au-emulsion data in the 10A GeV energy range, existence of a few particle correlations was established, which showed larger intermittency exponents in 2d than in 1d [38]. Evidence of a few-particle correlations was also found in the ^{32}S-Ag/Br interaction at 200A GeV and ^{28}Si-Ag/Br interaction at 14.5A GeV [21, 39]. These results

could not be explained either by the FRITIOF or by the UrQMD model. On the other hand, a partonic AMPT model grossly reproduced the ^{16}O-Ag/Br interaction data on the SFM at $E_{\rm lab} = 4.5A$, $14.5A$, $60A$ and $200A$ GeV (EMU01 experiment) [40].

The intermittency phenomenon has also been studied in leptonic (ll) and hadronic (hh) interactions at relativistic energies. The experiments on π^+p and K^+p collisions at $p_{\rm lab} = 250$ GeV/c (NA22 experiment) gave an evidence of intermittency in the rapidity space [41]. The results were compared with the FRITIOF-2.0, FRITIOF-3.0 and DPM models [42, 43]. The e^+e^- annihilation data at $\sqrt{s} = 29$ GeV [44] produced somewhat weaker intermittency than what was observed in hh interactions [41]. However, the strength of intermittency was found to be larger in ll interactions than in the AB collisions at a comparable collision energy. The above observation favors a jet cascading over a hadronic reaction mechanism as a possible interpretation of the intermittency phenomenon [41, 45, 46]. The UA1 collaboration [47] had also reported the results of intermittency analysis for the $\overline{p}p$ collisions at $\sqrt{s} = 630$ GeV. They showed that the quantitative measures of intermittency in different variables like η, y and φ are almost identical. The intermittency index increases with decreasing event multiplicity. A simple Monte Carlo model could not reproduce either the intermittency results for a sample of low p_T tracks, or its multiplicity dependence. The DELPHI experiment [48] showed that the rapidity scaling of SFMs in e^+e^- annihilation data at $\sqrt{s} = 91$ GeV is consistent with the JETSET-6.3 PS model prediction [49]. Intermittency of rapidity distributions in the e^+e^- annihilation data obtained from PEP and PETRA [44, 50, 51] was also examined in terms of a QCD bunching process [52]. The investigation suggests that for most of the observables the dynamics can be described by soft hadronization, and the perturbative gluon radiation is of lesser importance. In a three (y, p_t, φ) and two dimensional (y, p_t), (y, φ), (p_t, φ) analysis of the SFM on π^+p and K^+p interactions at $E_{\rm lab} = 250$ GeV (NA22 Collaboration) [53], an evidence of dimensional reduction in the intermittency strength was observed. It was also found that the density fluctuations in the final stages of these interactions are self-similar in the transverse plane, but self-affine in the longitudinal one. In AB collisions also, the intermittency exponent was reduced when projected from a higher to lower sub-dimensions [38].

The event space fluctuations of the SFMs are described by a set of moments called the erraticity moments [18]. The erraticity moments in AB, hadronic and leptonic collisions at relativistic energies were measured [18–20, 54–60]. Most of these results indicated the existence of event to event fluctuations, which for an integer order q, was quantified by a parameter called the entropy index μ_q. The NA27 data on pp collisions at 400 GeV showed an increase in μ_q with decreasing average multiplicities of the final state particles [58]. The experimental observation was close to the prediction of a Monte-Carlo simulation based on the quark jets which used a very small fixed coupling constant α_s [61]. The same erraticity

results of the NA27 experiment could be explained also by a purely statistical model that used the negative binomial multiplicity distribution [62]. However, a soft-interaction model called the ECOMB, was unable to describe the NA22 results on e^+e^- collision [41, 63], and NA27 results on pp collision [20]. The erraticity results on π^+p and K^+p collisions at 250 GeV/c (NA22 Collaboration) [64] were compared with the PYTHIA 5.720 model [65]. The erratic nature of event to event fluctuations in the data could not be matched by PYTHIA 5.720, and the erraticity moments are found to be dominated by statistical noise [66].

The multiplicity dependence of the erraticity parameters are observed in ^{28}Si-nucleus interactions at 4.5A and 14.5A GeV/c [67, 68]. It was found that the magnitude of erraticity moments decreased with increasing multiplicity and were essentially insensitive to the incident beam energy and mass of the beam/target nuclei [66]. A comparison of these results with those reported by other experiments [55–57], suggested that the erratic fluctuations present in the data were due to statistical reasons, and no unambiguous evidence of dynamical fluctuations could be established. The results more or less matched with the prediction of the FRITIOF model. However, FRITIOF could not account for the observed erraticity measures in ^{16}O-Ag/Br and ^{32}S-Ag/Br interactions at 200A GeV [22], indicating the presence of dynamical components in the erraticity measures. A comparison of the results of [23] with those obtained from the ECOMB-generated hadronic events [20], as well as with the results obtained from other experiments [58, 59, 69] showed that, the erraticity parameters were significantly smaller in the ^{32}S-Ag/Br experiment than those obtained from other experiments at a similar energy. The entropy index was calculated for the target fragments emitted in the ^{32}S-Ag/Br interaction at 200A GeV (CERN SPS) and ^{28}Si-Ag/Br interaction at 14.5A GeV (BNL AGS). The results were in conformity with the chaotic behavior of target fragmentation. For the ^{28}Si-data the entropy index was much greater ($\sim$ 2.6 times) than that for the ^{32}S-data [70]. Moreover the entropy indices in the target fragmentation region showed an increasing trend with an increase in the charged particle multiplicity [59, 60, 71, 72].

3.3 Scaled factorial moments

We know that a statistical distribution can be characterized by its moments. For a given discrete probability distribution P_n ($n = 1, 2, \cdots$) the ordinary q-th order moment is obtained as,

$$\langle n^q \rangle = \sum_{n=0}^{\infty} n^q \, P_n \;\; : \qquad \text{for } q = 0, 1, 2, \cdots \tag{3.2}$$

The event averaged q-th order factorial moment (FM) on the other hand is defined as,

$$\langle f_q \rangle = \left\langle n^{[q]} \right\rangle = \langle n(n-1)\cdots(n-q+1) \rangle \tag{3.3}$$

Here n represents the frequency (number of particles) of an arbitrary phase space interval, and $\langle\ \rangle$ denotes that the quantity is averaged over the event sample. In terms of the inclusive distribution $\rho_q(y_1, y_2, \cdots, y_q)$ for q particles in the variable y over a domain Ω, the FMs is given by

$$\langle f_q \rangle = \int_\Omega dy_1 \cdots \int_\Omega dy_q\, \rho_q(y_1, y_2, \cdots, y_q) \tag{3.4}$$

The normalized or scaled factorial moment (SFM) is defined as,

$$\begin{aligned} F_q &= \frac{\int_\Omega dy_1 \cdots \int_\Omega dy_q\, \rho_q(y_1, y_2, \cdots, y_q)}{\left[\int_\Omega dy \rho_1(y)\right]^q} \\ &= \frac{\sum_{n=0}^{\infty} n(n-1)\cdots(n-q+1)P_n}{\langle n \rangle^q} \end{aligned} \tag{3.5}$$

Whereas the ordinary moments cannot eliminate the statistical components of the fluctuations, the factorial moments can take care of Poisson type noise. For instance, in an arbitrary bin having a multiplicity n, if we denote the dynamical component by $D(t)$ then,

$$P_n = \int_0^\infty \frac{t^n}{n!}\, e^{-t}\, D(t)\, dt \tag{3.6}$$

For a large event sample the bin-multiplicity n can run from zero to a very large value, effectively infinity. Therefore,

$$\begin{aligned} \langle f_q \rangle &= \sum_{n=0}^{\infty} n(n-1)\cdots(n-q+1)P_n = \sum_{n=q}^{\infty} \frac{n!}{(n-q)!} P_n \\ &= \sum_{n=q}^{\infty} \int_0^\infty \frac{t^n}{(n-q)!}\, e^{-t} D(t)\, dt \\ &= \int_0^\infty t^q\, D(t)\, dt \end{aligned} \tag{3.7}$$

This shows that $\langle f_q \rangle$ is identical to the ordinary q-th order moment of the dynamical component of the distribution, and Poisson type statistical fluctuations can be successfully eliminated. The normalization property of the Poission distribution is employed in the above derivation. A detailed discussion on multiplicity moments, especially those related to the multiparticle emission physics, can be found in [1, 73]. The idea of [6] was to study the structure of particle density in rapidity or any other suitable phase space variable. We may consider the pseudorapidity (η) variable for our discussion. It can been shown that the SFM averaged over M sub-intervals, each of width $\delta\eta$ considered within an acceptance

$\Delta\eta = M\delta\eta$, corresponds to the moment of the probability density in those bins. Based on the normalization method adopted, the SFM is said to be a *horizontally averaged* or a *vertically averaged* factorial moment [7]. In terms of the inclusive distribution $\rho_q(\eta)$ the horizontally averaged SFM is defined as,

$$\begin{aligned} F_q^H(\eta) &= \frac{1}{M}\sum_{m=1}^{M}\frac{\int_{\delta\eta}\rho_q(\eta_1,\ldots,\eta_q)\prod_{i=1}^{q}d\eta_i}{\left(\int_{\delta\eta}\rho(\eta)d\eta/M\right)^q} \\ &= \frac{1}{M}\sum_{m=1}^{M}\frac{\left\langle n_m^{[q]}\right\rangle}{\langle\bar{n}_m\rangle^q} \end{aligned} \tag{3.8}$$

where $\langle\bar{n}_m\rangle = \langle n\rangle/M$, $n = \sum_m n_m$ is the total number of particles present within $\Delta\eta$ in an event. The vertically averaged SFM on the other hand is defined as,

$$\begin{aligned} F_q^V(\eta) &= \frac{1}{M}\sum_{m=1}^{M}\frac{\int_{\delta\eta}\rho_q(\eta_1,\cdots,\eta_q)\prod_{i=1}^{q}d\eta_i}{\left(\int_{\delta\eta}\rho(\eta)d\eta\right)^q} \\ &= \frac{1}{M}\sum_{m=1}^{M}\frac{\left\langle n_m^{[q]}\right\rangle}{\langle n_m\rangle^q} \end{aligned} \tag{3.9}$$

Here $\langle n_m\rangle$ is the number of particles in the m-th bin averaged over the event sample. Both the moments F_q^H and F_q^V scale with phase space resolution size ($\delta\eta$) or equivalently with the partition number (M) like,

$$F_q^s \sim M^{\phi_q} \quad \text{for large} \;\; M \tag{3.10}$$

where $s = H$ or V. Irrespective of the averaging technique adopted, the SFM is capable of suppressing any Poission distributed statistical noise. The vertically averaged SFMs are more sensitive to the bin-to-bin density variations but they are unstable at small bin sizes. Whereas the horizontally averaged SFMs are sensitive only to the local fluctuations of the particle density, but they remain stable over a large $\delta\eta$-range. Both the moments are equal for $M = 1$ and also when the underlying distribution in the particular phase space variable is uniform. The latter criterion is achieved by using a cumulant variable X_η defined as [74]

$$X_\eta = \int_{\eta_{\min}}^{\eta}\rho(\eta)d\eta \Big/ \int_{\eta_{\min}}^{\eta_{\max}}\rho(\eta)d\eta \tag{3.11}$$

where $\eta_{\min}$ ($\eta_{\max}$) is the minimum (maximum) value of η, and the single particle inclusive density in η is $\rho(\eta) = N_{ev}^{-1}(dn/d\eta)$. Irrespective of its original form, density distribution in terms of X_η is always uniform $\in [0,1]$. The present analysis is based on the distributions of cumulant variables corresponding to the η and/or φ variables. We shall however continue to call the corresponding variables η and φ.

3.3.1 Intermittency in $1d$

We compute the event averaged SFMs denoted by $\langle F_q \rangle$ as functions of phase space partition number M for the ^{16}O-Ag/Br interaction at 200A GeV/c. Figure 3.1 shows our results in the η-space and Figure 3.2 in the φ-space. In both the figures we include the results obtained from the UrQMD and UrQMD+BEC simulations. We find that the event averaged SFMs for $q = 2$ to 6 obey a power law type scaling relation like Equation (3.10), indicating an intermittent pattern of particle density functions in both the η and φ spaces. The straight

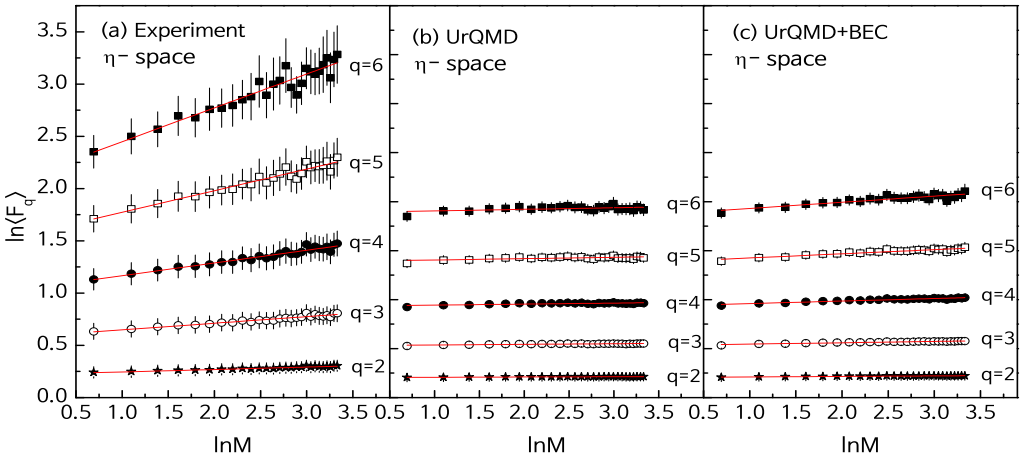

Figure 3.1: Variation of the event averaged SFM of shower tracks with phase space partition number M in the η-space for the ^{16}O-Ag/Br interaction at 200A GeV/c. Best fitted straight lines to the data points are shown.

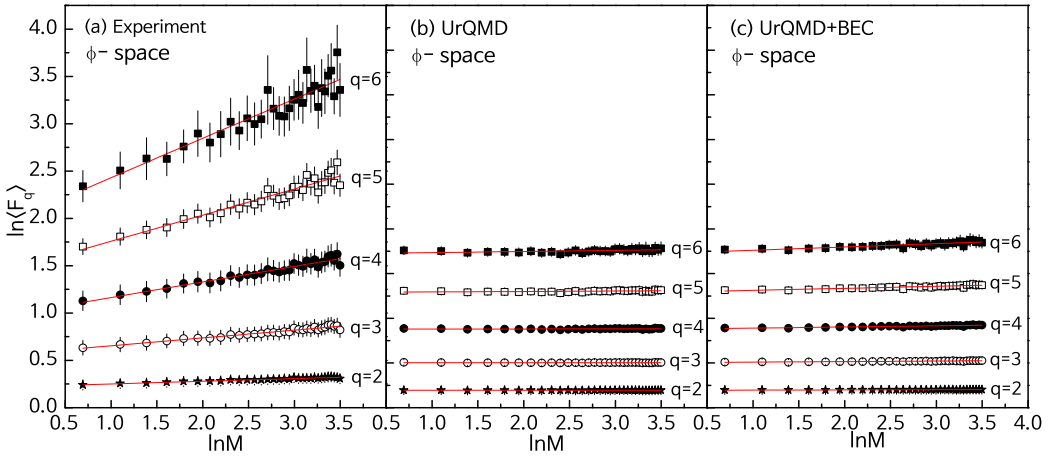

Figure 3.2: Same as in Figure 3.1 but in φ-space.

lines in these figures represent the best fitted scaling function of Equation (3.10) with ϕ_q as a free parameter. The ϕ_q exponents called the *intermittency index*, are given in Table 3.1. In order to avoid the kinematic constraints [75] a few points at the lowest values of M are

excluded while fitting the straight lines. We have also computed the $1d$ intermittency exponents for the ^{32}S-Ag/Br interaction at $200A$ GeV/c, and the values are given in Table 3.2. The diagrams as well as the tables suggest that the intermittency exponents are significantly larger in the experiments than in the simulations. The UrQMD+BEC generated values of ϕ_q are slightly larger than the corresponding UrQMD generated values. The errors associated with ϕ_q are estimated by assuming that for each event F_q is an error free quantity. Thus the standard error in $\langle F_q \rangle$ originates only from the event space fluctuation of the SFM. At this point it should be mentioned that, as the SFMs are computed in the same domain $(\Delta\eta)$ with varying bin size $(\delta\eta)$, in Figure 3.1 and Figure 3.2 for a given q the data points are highly correlated. Thus the error estimation of ϕ_q requires special precaution [76]. We have generated 10 independent samples, each equal in size as the respective experimental sample, by using the Lund model FRITIOF [77]. Gross characteristics of the data like the multiplicity and η-distribution of each FRITIOF generated sample are identical to the respective experiment. We then calculate ϕ_q for each FRITIOF generated sample and obtain their statistical spread as,

$$\sigma(\phi_q) = \sqrt{\langle \phi_q^2 \rangle - \langle \phi_q \rangle^2} \tag{3.12}$$

over the 10 sets of MC data used. The $\sigma(\phi_q)$ values obtained in this way are quoted as errors of ϕ_q in the η-space. For the error estimation in φ-space we follow the same procedure, but the FRITIOF data are now replaced by (pseudo)random numbers $\in [0, 2\pi]$. Since the FRITIOF model as well as the random number generated samples contain either none or very little dynamical effect, the estimated errors of the intermittency exponents are only of statistical origin. The goodness of linear regression is represented by the Pearson's coefficient (R^2) [78]. In almost all the cases the R^2 values are very close to unity, confirming the linearity of $\ln F_q$ with $\ln M$. We see that the intermittency indexes in the φ-space are higher in magnitude than those in the η-space. Such a phase space dependence of the intermittency index is found to be valid for both the ^{16}O-Ag/Br and ^{32}S-Ag/Br interactions, and is consistent with our previous observation for the ^{28}Si-Ag/Br interaction at $14.5A$ GeV as well [79]. The findings of our analysis however contradict the observation of [76], where a phase space independence was observed in this regard. We also find that the ϕ_q values in the ^{16}O-Ag/Br interaction are 2 to 3 times larger in magnitude than those in the ^{32}S-Ag/Br interaction, which might be an effect of projectile mass difference. It is found that at comparable energies the intermittency indices in leptonic and hadronic interactions are higher in magnitude than those in the AB interactions [41, 44, 50, 53, 80]. One may argue that due to intermixing of many particle producing sources, the correlations coming from elementary NN interactions are to some extent washed out, and the intermittency phenomenon in AB collisions is therefore partially suppressed [81]. For both the systems studied in this investigation, the UrQMD generated data do not produce intermittency. The SFMs are almost independent of the phase space partition number. Alternatively, we can say

that the model does not generate enough dynamical fluctuation. The inclusion of BEC into the UrQMD generated events introduces only a small but finite amount of correlation that is visible in the figures as well as in the tables. To check whether the observed intermittency effects are due to the contributions coming from lower order correlations, for $q \geq 2$ we define a set of normalized exponents ξ_q as [76],

$$\xi_q = \phi_q / \binom{q}{2} \tag{3.13}$$

A true three-particle correlation is then given by,

$$\xi_q^{(3)} = (q-2)\xi_3 - (q-3)\xi_2 \tag{3.14}$$

In Figure 3.3 we show the variations of ξ_q and $\xi_q^{(3)}$ with q in both η and φ-space for the ^{16}O-Ag/Br interaction, whereas similar diagrams for the ^{32}S-Ag/Br interaction are shown in Figure 3.4. In these diagrams the experimental results are compared with the corresponding UrQMD and UrQMD+BEC simulations. For the ^{16}O-Ag/Br experiment the normalized three-particle correlation parameter $\xi_q^{(3)}$ is seen to linearly decrease with increasing q. In the φ-space $\xi^{(3)}$ is consistently higher than that in the η-space. Corresponding UrQMD and UrQMD+BEC simulated results are significantly smaller than the experiment. In φ-space the UrQMD simulated values of $\xi^{(3)}$ are very close to zero. On the other hand, for the ^{32}S-Ag/Br experiment the $\xi_q^{(3)}$ values in the φ-space are not only larger in magnitude than those in the η-space, but they are also found to linearly rise with increasing q. In the

Table 3.1: The values of $1d$ intermittency exponent for order $q = 2-6$ in the ^{16}O-Ag/Br interaction at $200A$ GeV/c. The errors are of statistical origin.

		η-space		φ-space	
	Order	ϕ_q	R^2	ϕ_q	R^2
Experiment	2	0.0289±0.0011	0.939	0.0333±0.0002	0.984
	3	0.0779±0.0022	0.935	0.0972±0.0014	0.951
	4	0.1534±0.0061	0.930	0.1925±0.0038	0.945
	5	0.2534±0.0103	0.927	0.3172±0.0047	0.947
	6	0.3771±0.0167	0.915	0.4618±0.0081	0.918
UrQMD	2	0.0026±0.0003	0.979	-0.0002±0.0002	0.931
	3	0.0063±0.0008	0.932	-0.0001±0.0005	0.931
	4	0.0101±0.0018	0.947	0.0016±0.0011	0.931
	5	0.0136±0.0034	0.921	0.0052±0.0020	0.923
	6	0.0162±0.0060	0.975	0.0126±0.0037	0.925
UrQMD+BEC	2	0.0052±0.0003	0.956	0.0022±0.0002	0.907
	3	0.0136±0.0008	0.958	0.0062±0.0005	0.913
	4	0.0259±0.0017	0.949	0.0130±0.0011	0.908
	5	0.0423±0.0032	0.934	0.0231±0.0022	0.990
	6	0.0630±0.0060	0.907	0.0371±0.0390	0.964

Table 3.2: The values of $1d$ intermittency exponent for order $q = 2 - 6$ in ^{32}S-Ag/Br interaction at 200A GeV/c. The errors are of statistical origin only.

		η-space		φ-space	
	Order	ϕ_q	R^2	ϕ_q	R^2
Experiment	2	0.013±0.003	0.982	0.014±0.0006	0.967
	3	0.032±0.003	0.977	0.044±0.002	0.972
	4	0.056±0.007	0.961	0.099±0.005	0.967
	5	0.082±0.013	0.937	0.201±0.011	0.946
	6	0.112±0.021	0.905	0.371±0.021	0.915
UrQMD	2	0.001±0.0001	0.986	0.012±0.0006	0.953
	3	0.004±0.0004	0.939	0.033±0.0015	0.956
	4	0.009±0.0008	0.946	0.062±0.0027	0.958
	5	0.017±0.0017	0.930	0.097±0.0042	0.959
	6	0.032±0.0035	0.999	0.138±0.0061	0.957
UrQMD+BEC	2	0.002±0.0002	0.953	0.029±0.0009	0.976
	3	0.005±0.0005	0.952	0.078±0.0025	0.967
	4	0.009±0.0010	0.920	0.143±0.0045	0.987
	5	0.016±0.0021	0.955	0.224±0.0073	0.975
	6	0.026±0.0042	0.969	0.323±0.0113	0.972

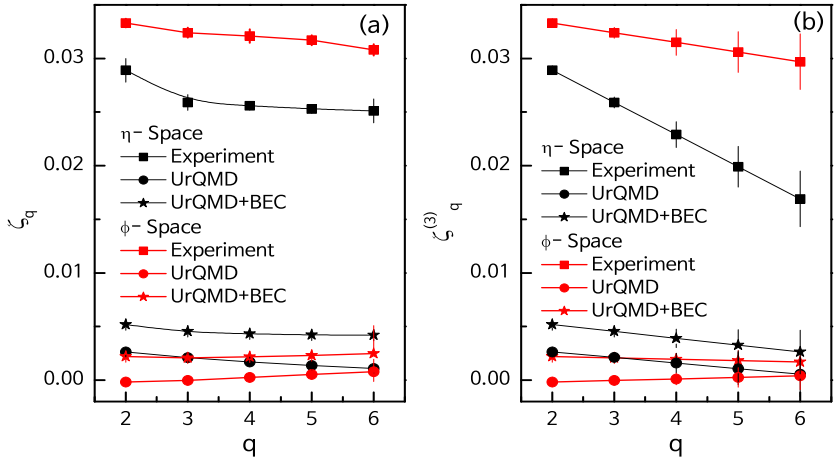

Figure 3.3: Normalized intermittency exponents as a function of order number q for the ^{16}O-Ag/Br interaction at 200A GeV/c. Lines joining points are drawn to guide the eye.

η-space the UrQMD and UrQMD+BEC simulated $\xi_q^{(3)}$ values both are again very close to zero. However, in the φ-space very surprisingly the UrQMD+BEC simulation significantly exceeds the experiment until $q = 6$. The overall observation indicates that the higher order ($q \geq 2$) intermittency present in the experiments cannot simply be explained in terms of the lower order two and three-particle correlations.

A self-similar cascade mechanism may occur in different phases, leading to different kinds of spiky events. In some events there are many spikes, such as in the JACEE events [8], while in some other only one or two large spikes are seen [82]. In high-energy AB interactions when

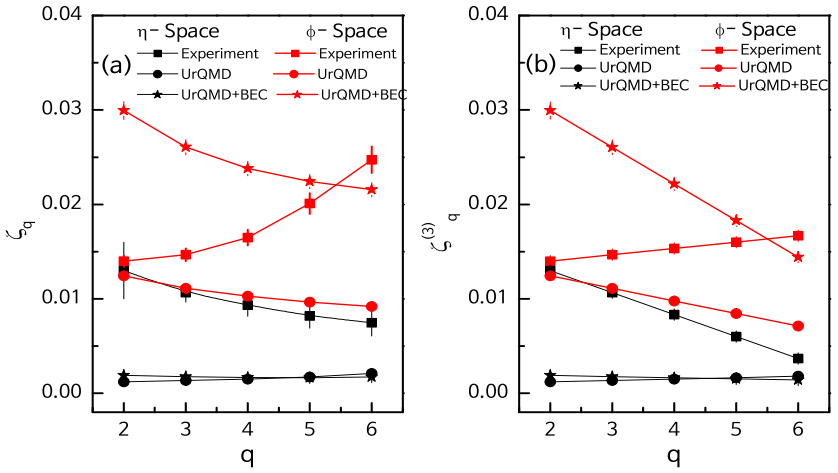

Figure 3.4: The same as in Figure 3.3 but for the ^{32}S-Ag/Br interaction at 200A GeV/c.

the normal hadronic phase dominates, the events are populated by many spikes and valleys. On the other hand, a few large spikes are observed in events dominated by a spin-glass like phase. If the two phases are simultaneously present, then the parameter

$$\lambda_q = (\phi_q + 1)/q \tag{3.15}$$

should exhibit a minimum at a certain order number q, say at $q = q_c$, that is not necessarily an integer [11]. In the region $q < q_c$ a self-similar multiparticle system would behave differently from that in the $q > q_c$-region. Whereas the $q < q_c$-region is dominated by numerous fluctuations involving smaller numbers of particles in one bin, the $q > q_c$-region is dominated by a small number of very large fluctuations [83]. The situation can be described as a mixture of a *liquid phase* of many small fluctuations and a *dust phase* of a few grains of very large fluctuations. The liquid-dust phases can coexist. However, when the system was examined by using moments of rank $q < q_c$ and $q > q_c$, one found that either the *liquid* or the *dust* phase dominates [11]. In Figure 3.5(a) and Figure 3.6(a) we have plotted λ_q against q, respectively for the ^{16}O-Ag/Br and ^{32}S-Ag/Br interactions at 200A GeV/c. In both diagrams the experimental results are shown along with the respective UrQMD and UrQMD+BEC simulations. The figures show that the experimental values of λ_q in both η and φ-space deviate to a small extent from the respective no-intermittency lines. The simulated values of λ_c on the other hand are always very close to the no-intermittency line. According to [84] the observed q-dependence represents a weak $1d$ intermittency in the experiment(s). It may be noted that the deviation from the no-intermittency line is slightly larger in φ-space than what it is in the η-space.

A more direct measure of the intermittency strength can be obtained from its connection with (multi)fractality, at first in the framework of the α-model [7], and subsequently in a

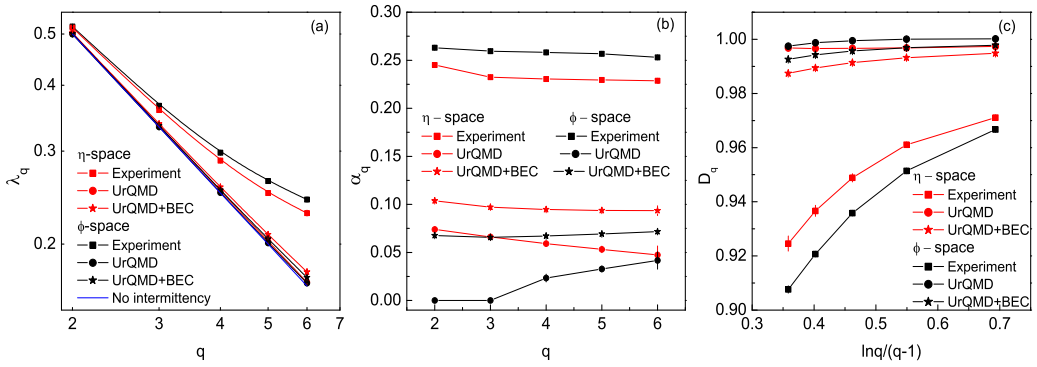

Figure 3.5: (a) Plot of λ_q versus q. The no-intermittency line corresponding to $\phi_q = 0$ is also shown. (b) Plot of intermittency strength α_q with q. (c) Plot of generalized Rényi dimension D_q with $\ln q/(q-1)$. The curves are drawn to guide the eye. The plots are for the ^{16}O-Ag/Br interaction at 200A GeV/c.

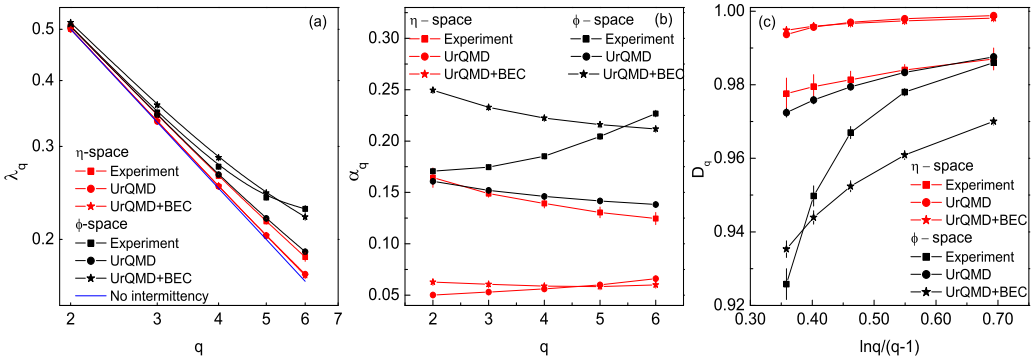

Figure 3.6: The same as in Figure 3.5 but for the ^{32}S-Ag/Br interaction at 200A GeV/c.

model independent way that does not invoke any particular hypothesized mechanism of particle production [85]. The generalized Rényi dimension of multifractality can be determined from the intermittency exponent ϕ_q by using the following relation,

$$D_q = D_T - \frac{\phi_q}{(q-1)} \tag{3.16}$$

where D_T is the topological dimension of the supporting space, i.e. $D_T = 1\,(2)$ in a $1d\,(2d)$ analysis. According to the α-model the strength parameter α_q is related to D_q as,

$$\alpha_q = \sqrt{\frac{6\ln 2}{q}(D_T - D_q)} \tag{3.17}$$

The α_q parameter as a function of q is plotted in Figure 3.5(b) for the ^{16}O-Ag/Br interaction and in Figure 3.6(b) for the ^{32}S-Ag/Br interaction. In the ^{16}O-Ag/Br interaction

the experimental values of $\alpha_q \approx 0.25$ and they are almost independent of q, whereas the simulated α_q-values are found to vary in the $0 - 0.1$ range. The α_q against q plots for the ^{32}S-Ag/Br interaction are quite different. In the experiment α_q increases in the φ-space and decreases in the η-space. Once again the UrQMD+BEC simulated values of the parameter are significantly larger than those of the experiment in the $q = 2$ to 5 range. From the above discussion it cannot be claimed in clear terms as to which process, i.e. a second-order phase transition or a random cascading, is actually responsible for the intermittency observed in the experiments. For an arbitrary underlying dynamics it is however possible to define an effective fluctuation strength as [85],

$$\alpha_{\text{eff}} \propto \sqrt{2\phi_2} \tag{3.18}$$

The values of α_{eff} are found to be $\alpha_{\text{eff}}(\eta) = 0.240 \pm 0.005$ and $\alpha_{\text{eff}}(\varphi) = 0.258 \pm 0.0008$ for the ^{16}O-Ag/Br experiment, and $\alpha_{\text{eff}}(\eta) = 0.161 \pm 0.019$ and $\alpha_{\text{eff}}(\varphi) = 0.167 \pm 0.004$ for the ^{32}S-Ag/Br experiment.

Table 3.3: Multifractal specific heat C calculated from the SFM analysis. The C values evaluated at different q-regions are specified.

Interaction		Fit Region	η-space	φ-space
^{16}O-Ag/Br	Experiment	2≤q≤5	0.1148±0.0199	0.1540±0.0214
interaction		2≤q≤4	0.0936±0.0186	0.1309±0.0192
at 200A GeV/c		4≤q≤6	0.2324±0.0195	0.2707±0.0122
	UrQMD	2≤q≤5	0.0028±0.0004	0.0047±0.0017
		2≤q≤4	0.0032±0.0003	0.0028±0.0015
		4≤q≤6	-0.0011±0.0012	0.0188±0.0041
	UrQMD+BEC	2≤q≤5	0.0179±0.0030	0.0118±0.0025
		2≤q≤4	0.0146±0.0025	0.0089±0.0021
		4≤q≤6	0.0380± 0.0039	0.0294±0.0036
^{32}S-Ag/Br	Experiment	2≤q≤5	0.0257± 0.0019	0.1161± 0.0313
interaction		2≤q≤4	0.0242± 0.0026	0.0796± 0.0188
at 200A GeV/c		4≤q≤6	0.0357± 0.0035	0.3909±0.0715
	UrQMD	2≤q≤5	0.0102± 0.0022	0.0394±0.0045
		2≤q≤4	0.0077±0.0015	0.0345±0.0040
		4≤q≤6	0.0310±0.0064	0.0673±0.0047
	UrQMD+BEC	2≤q≤5	0.0073±0.0010	0.0875±0.0111
		2≤q≤4	0.0061±0.0007	0.0751±0.0089
		4≤q≤6	0.0177± 0.0034	0.1634±0.0149

A thermodynamic interpretation of multifractality has been given in terms of a constant specific heat C that is related to the Rényi dimension as [86],

$$D_q = D_\infty + C\,\frac{\ln q}{q-1} \tag{3.19}$$

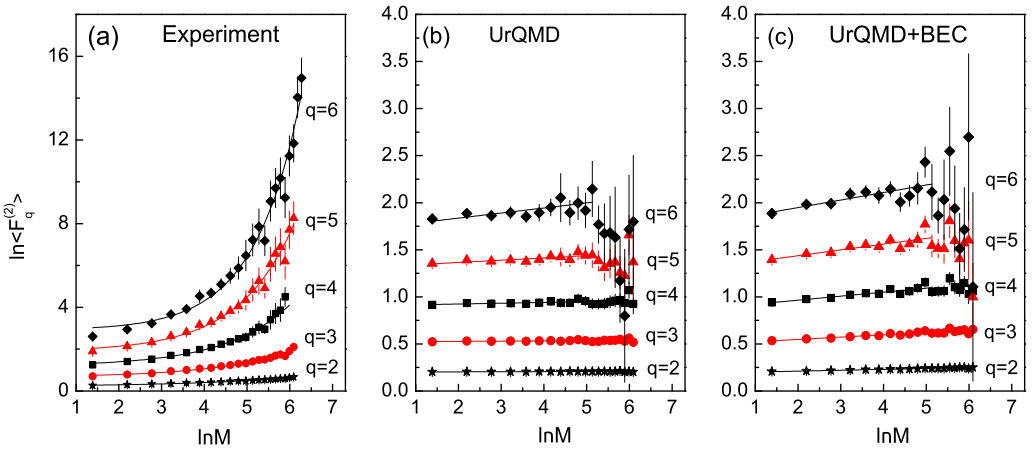

Figure 3.7: The scaling of $2d$ SFMs for $q = 2-6$ in ^{16}O-Ag/Br interaction at 200A GeV/c. The solid curves are drawn to guide the eye.

While deriving the above relation it has been assumed that only Bernoulli type of fluctuations are responsible for a transition from monofractality to multifractality. A monofractal to multifractal transition corresponds to a jump in the value of C from zero to a nonzero positive value. By examining the variation of D_q with $\ln q/(q-1)$ one can obtain the value of C. Such results for our investigation are shown in Figure 3.5(c) for the ^{16}O-Ag/Br interaction and in Figure 3.6(c) for the ^{32}S-Ag/Br interaction. The experimental values of D_q increase nonlinearly with increasing $\ln q/(q-1)$. For both interactions the nonlinearity in φ-space is more prominent than that in the η-space. The C value will obviously depend on the order number q. The simulated values in all cases are very close to unity, the topological dimension of the supporting space. We have computed C in three different domains of q. Table 3.3 summarizes our results. It shows that the C values obtained from the experimental data are always positive. The simulated values are very close to zero or at least about an order less than the corresponding experimental values. We also observe that the values of C are not consistent with the universality of the parameter as claimed in [86].

3.3.2 Intermittency in $2d$

In a $2d$ analysis of intermittency we consider the (η, φ)-plane as our phase space. In order to make the results independent of the underlying distribution functions, the cumulative variables (X_η, X_φ) have been used [74]. Therefore, all the particles are distributed uniformly over a square of unit side. The q-th order SFM is calculated following Equation (3.8), where the phase space partition number is taken as $M = M_\eta \cdot M_\varphi$, and M_η (M_φ) is the number of partitions along the η (φ) direction. For a self-similar structure the $2d$-SFMs are expected to follow a scaling relation like Equation (3.10) in the (η, φ)-plane. In Figure 3.7 we show the plots of event averaged $2d$ SFMs $\langle F_q^{(2)} \rangle$ against M for the ^{16}O-Ag/Br data. Here we have set

Table 3.4: $2d$ self-affine intermittency indices for the ^{16}O-Ag/Br interaction at 200A GeV/c. The errors are statistical only.

	Experiment		UrQMD		UrQMD+BEC	
q	$\phi_q^{(2)}$	R^2	$\phi_q^{(2)}$	R^2	$\phi_q^{(2)}$	R^2
2	0.125±0.025	0.994	0.001±0.0004	0.476	0.009±0.0004	0.983
3	0.339±0.045	0.987	0.002±0.001	0.218	0.025±0.003	0.909
4	0.857±0.115	0.983	0.008±0.004	0.316	0.043±0.008	0.759
5	1.596±0.198	0.986	0.024±0.006	0.643	0.061±0.016	0.589
6	3.059±0.270	0.983	0.054±0.018	0.467	0.080±0.026	0.494

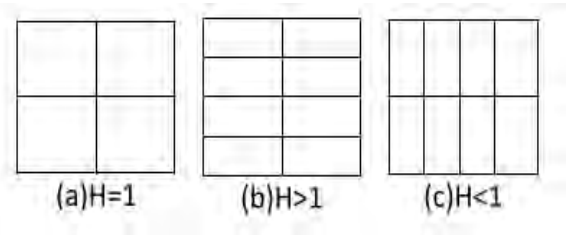

Figure 3.8: A schematic of partitioning $2d$ phase space for (a) $H = 1$ corresponds to equal partitioning, (b) $H > 1$ corresponds to finer division along the vertical direction, and (c) $H < 1$ corresponds to finer division along the horizontal direction.

$M_\eta = M_\varphi$ which corresponds to a self-affine partitioning of the phase space. The experiment, UrQMD and UrQMD+BEC generated results are plotted together in this figure. Due to the anisotropy present in the fluctuations in two different directions (i.e., a self-affine structure) of phase space, the variation of $\ln\langle F_q^{(2)}\rangle$ against $\ln M$ is not linear over the entire $\ln M$ range. To obtain a measure of the self-affine intermittency index in $2d$ one can perform a polynomial fit to the $\ln\langle F_q^{(2)}\rangle$ versus $\ln M$ data, and then retain only the linear coefficient by setting all other coefficients zero. For the ^{16}O-Ag/Br interaction the $2d$ self-affine intermittency index $\phi_q^{(2)}$ obtained in this way is presented in Table 3.4. Once again the fit quality is measured by the Pearson's coefficient R^2 [78] and their values are quoted in Table 3.4. The same set of exponents for the ^{32}S-Ag/Br interaction at 200A GeV/c are given in Table 3.5. The errors quoted in these tables are only of statistical origin. The procedure of error estimation is

Table 3.5: $2d$ self-affine intermittency indices for the ^{32}S-Ag/Br interaction at 200A GeV/c. The errors are statistical only.

	Experiment		UrQMD		UrQMD+BEC	
q	$\phi_q^{(2)}$	R^2	$\phi_q^{(2)}$	R^2	$\phi_q^{(2)}$	R^2
2	0.075±0.003	0.974	0.003±0.0002	0.978	0.009±0.0003	0.996
3	0.384±0.038	0.984	0.009±0.001	0.974	0.026±0.0009	0.993
4	1.030±0.170	0.969	0.017±0.003	0.967	0.048±0.002	0.985
5	1.560±0.290	0.946	0.026±0.003	0.944	0.072±0.006	0.960
6	2.022±0.099	0.958	0.049±0.004	0.983	0.103±0.009	0.977

similar to that used in our $1d$ intermittency analysis. It is seen that the $2d$ intermittency exponents for the UrQMD and UrQMD+BEC simulations are comparatively lower valued than the corresponding experiment. For a given q the ^{16}O-Ag/Br experiment produces larger $\phi_q^{(2)}$ value than the ^{32}S-Ag/Br experiment. The $\alpha_q^{(2)}$ values for the ^{16}O-Ag/Br experiment increase with increasing q, but for the ^{32}S-Ag/Br experiment the values initially rise and then saturate near $q = 4$. It has been conjectured [10, 87] that beside some kind of collective phenomena there are other possibilities, e.g. a branching process or a second order phase transition, that lead to the $2d$ intermittency within a scale invariant dynamics. To check whether or not these mechanisms are acceptable in the present analysis for our ^{16}O-Ag/Br and ^{32}S-Ag/Br data, the $\phi_q^{(2)}$ values, shown in Table 3.4 and Table 3.5, are put to different tests. Our observations in this regard are listed below.

(i) Unlike the $1d$ intermittency exponents the $\phi_q^{(2)}$ values do not follow the predictions of a self-similar cascade mechanism. Neither a log-normal distribution under Gaussian approximation [6, 7] nor a log-Lévy stable distribution works for the observed values [88, 89], thereby ruling out a self-similar cascade process in $2d$. The Rényi dimensions, shown in Table 3.6, are however fractional valued and decrease with increasing q, which indicates a (multi)fractal nature of the underlying dynamical fluctuation.

(ii) The intermittency parameter λ_q obtained from $\phi_q^{(2)}$ does not exhibit any clear minimum. Hence the possibility of coexistence of two different phases (e.g., liquid-gas) is also ruled out for both ^{16}O-Ag/Br and ^{32}S-Ag/Br interactions at $200A$ GeV/c.

(iii) For both interactions the $\phi_q^{(2)}$ values are not consistent with a monofractal structure of particle production either, as required by a system at the critical temperature for a second order phase transition [90]. The Landau-Ginzburg parameter ν is also significantly different from its universal value ($\nu = 1.304$) to warrant any kind of thermal (second order) phase transition [91].

Following Equation (3.17) we determine the $2d$ intermittency strength $\alpha_q^{(2)}$ for the ^{16}O-Ag/Br and ^{32}S-Ag/Br interactions, and their values are given in Table 3.6. From the values of $\alpha_q^{(2)}$ and the plots of $1d$ intermittency strength shown in Figure 3.5 and Figure 3.6, one can conclude that the fluctuation strength in ^{16}O-Ag/Br interaction is consistently greater than that in the ^{32}S-Ag/Br interaction. We also observe that $\alpha_q^{(2)} > 2\alpha_q$. Nonlinearity in the partition number dependence of the $2d$ SFMs, as observed in Figure 3.7, is due to an anisotropy present in the (η, φ) plane. For a particular interaction the kinemtically allowed η-range depends on the collision energy and/or momentum, whereas the φ range irrespective of the colliding system and/or collision energy lies always in between 0 and 2π. It is therefore suggested that the phase space should be so partitioned as to appropriately

Table 3.6: Intermittency strength based on a random cascading α-model and Rényi dimensions for ^{16}O-Ag/Br and ^{32}S-Ag/Br interactions in $2d$. The errors are of statistical origin.

	^{16}O-Ag/Br		^{32}S-Ag/Br	
Order(q)	$D_q^{(2)}$	$\alpha_q^{(2)}$	$D_q^{(2)}$	$\alpha_q^{(2)}$
		Experiment		
2	1.875±0.025	0.487±0.006	1.925±0.003	0.395±0.006
3	1.831±0.023	0.502±0.012	1.808±0.039	0.516±0.010
4	1.714±0.038	0.549±0.032	1.657±0.057	0.597±0.051
5	1.601±0.049	0.612±0.063	1.610±0.073	0.570±0.083
6	1.388±0.054	0.643±0.084	1.596±0.020	0.528±0.106
		UrQMD		
2	1.999±0.0004	0.046±0.005	1.997±0.0002	0.079±0.001
3	1.999±0.0005	0.036±0.005	1.996±0.0005	0.079±0.002
4	1.997±0.001	0.053±0.007	1.994±0.001	0.077±0.003
5	1.994±0.002	0.071±0.004	1.994±0.001	0.074±0.002
6	1.989±0.004	0.087±0.007	1.990±0.001	0.082 ±0.002
		UrQMD+BEC		
2	1.991±0.0004	0.137±0.002	1.991±0.0003	0.137±0.001
3	1.988±0.002	0.132±0.004	1.987±0.0004	0.134±0.001
	1.986±0.003	0.122±0.006	1.984±0.0006	0.129±0.002
5	1.985±0.004	0.113±0.007	1.982±0.002	0.122 ±0.003
6	1.984±0.005	0.105±0.009	1.979±0.002	0.119±0.003

take this anisotropy into account [92]. This is usually done by introducing a *roughness* parameter called the Hurst exponent (H). A schematic of how H is related to the unequal partitioning of the (η, φ)-plane is shown in Figure 3.8. Following [93] we introduce H for an asymmetric partitioning of the (η, φ)-plane which is referred to as a self-affine structure of the phase space. The scale factors in different directions are related as,

$$M_\eta = M_\varphi^H : 0 < H < 1 \quad \text{and} \quad M_\varphi = M_\eta^{(1/H)} : H > 1 \tag{3.20}$$

Both M_η and M_φ now cannot be simultabeously integer valued. Therefore, one has to leave a small fraction out of our consideration along either η or φ-direction, as the case may demand. However, such exclusion is not going tp affect the final results, since the phase space variables X_η and X_φ are uniform $\in [0, 1]$. A self-affine analysis for $q = 2$ has been performed for a wide range of H values ($0.25 \leq H \leq 4.0$). Figure 3.9 illustrates the scaling of second order SFM $F_2^{(2)}$ for some selected values of H for the ^{16}O-Ag/Br interaction, while Figure 3.10 shows similar plots for the ^{32}S-Ag/Br interaction. From these figures one can see that as H differs from unity the phase space dependence of the $2d$ SFMs is gradually straightened out. For each H the $\langle F_2^{(2)} \rangle$ versus M data are fitted by the following quadratic equation,

$$y = ax^2 + bx + c \tag{3.21}$$

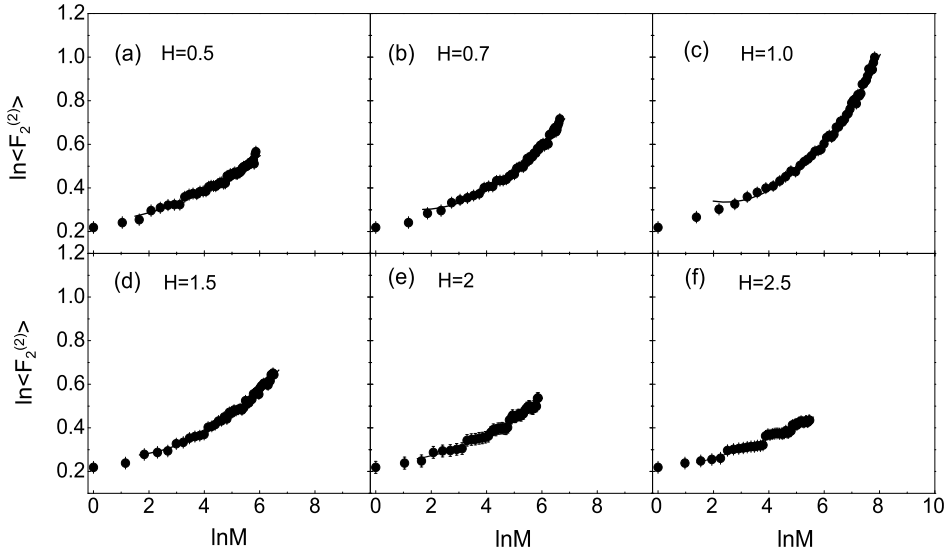

Figure 3.9: Two-dimensional SFM $\ln\langle F_2^{(2)}\rangle$ plotted against $\ln M$ for different Hurst parameters in the ^{16}O-Ag/Br interaction at 200A GeV/c. The solid curves represent quadratic fit to the data points.

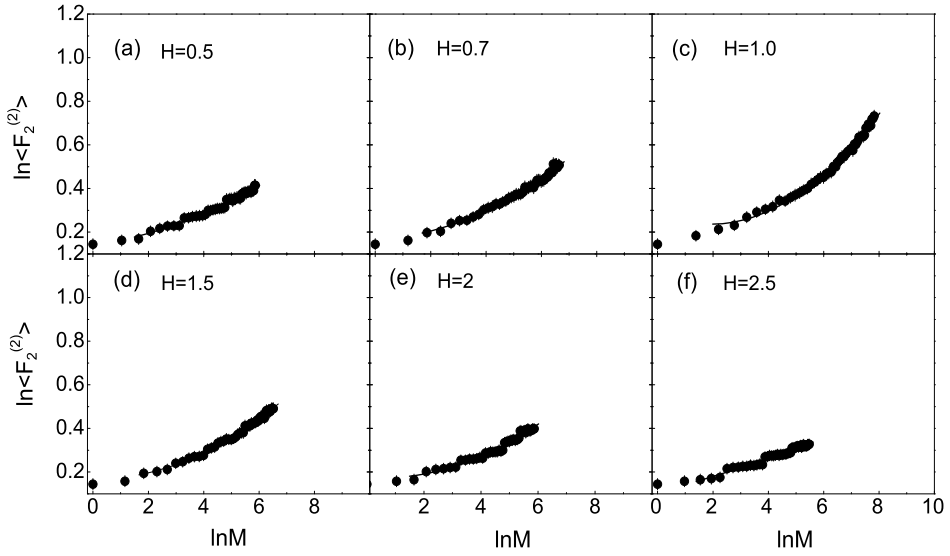

Figure 3.10: The same as in Figure 3.9 but for the ^{32}S-Ag/Br interaction at 200A GeV/c.

where $y = \ln\langle F_2^{(2)}\rangle$ and $x = \ln M$. In order to take care of the conservation rules depicted in [75] a couple of points at the lowest $\ln M$ region are omitted from the fits. Estimated values of the parameters a and b along with the R^2 coefficients are presented in Table 3.7 for the ^{16}O-Ag/Br interaction and in Table 3.8 for the ^{32}S-Ag/Br interaction. The errors quoted in these tables are statistical in nature. For both interactions the coefficient of the quadratic term in Equation (3.21) attains a maximum value at $H = 1.0$. Once the self-similarity of the underlying phase space is attained, one can estimate the effective fluctuation strength. A linear fit of the data as per Equation (3.10) now gives the required $\phi_q^{(2)}$ values at $H = 4.0$

Table 3.7: Values of fit parameters of $\ln\langle F_2^{(2)}\rangle$ against $\ln M$ plot by using a quadratic function like $f(x) = ax^2 + bx + c$ for the ^{16}O-Ag/Br interaction. The errors are of statistical origin.

Hurst Exponent(H)	a	b	R^2
0.25	0.0009±0.0021	0.0371±0.0144	0.908
0.30	0.0075±0.0025	-0.0016±0.0179	0.902
0.35	0.0021±0.0017	0.0376±0.0127	0.951
0.40	0.0034±0.0013	0.0319±0.0097	0.975
0.50	0.0073±0.0012	0.0066±0.0099	0.981
0.60	0.0111±0.0009	-0.0159±0.0086	0.990
0.70	0.0153±0.0010	-0.0491±0.0096	0.991
0.80	0.0184±0.0009	-0.0738±0.0095	0.993
1.0	0.0216±0.0010	-0.1051±0.0113	0.994
1.08	0.0182±0.0009	-0.0713±0.0104	0.994
1.1	0.0182±0.0010	-0.0712±0.0107	0.993
1.2	0.0154±0.0009	-0.0477±0.0100	0.992
1.4	0.0134±0.0008	-0.0335±0.0073	0.995
1.5	0.0122±0.0009	-0.0245±0.0084	0.992
1.6	0.0106±0.0009	-0.0106±0.0087	0.990
1.8	0.0092±0.0011	-0.0034±0.0093	0.986
2.0	0.0088±0.0013	-0.0053±0.0104	0.979
2.5	0.0039±0.0013	0.0223±0.0104	0.965
3.0	0.0055±0.0018	0.0068±0.0135	0.932
4.0	0.0006±0.0018	0.0309±0.0123	0.899

and 0.4, respectively for the ^{16}O-Ag/Br and ^{32}S-Ag/Br interactions. Note that the best linear dependence of $\ln\langle F_2^{(2)}\rangle$ on $\ln M$ is observed for the above specified values of H. We obtain the $2d$ intermittency index as $\phi_q^{(2)} = 0.0349 \pm 0.0017$ for the ^{16}O-Ag/Br interaction and $\phi_q^{(2)} = 0.0443 \pm 0.0012$ for the ^{32}S-Ag/Br interaction. The effective $2d$ intermittency strengths are $\alpha_{\rm eff}^{(2)} = 0.2642\pm0.0064$ for the ^{16}O-Ag/Br interaction and $\alpha_{\rm eff}^{(2)} = 0.2977\pm0.0040$ for the ^{32}S-Ag/Br interaction.

3.4 Factorial correlators

Factorial correlator (FC) introduced by Bialas and Peschanski [6, 7] is an important addition to the intermittency analysis of single particle density fluctuations. FCs can measure the local density fluctuations along with the bin-to-bin correlations present in the SFMs. The FCs are calculated for each combination of non-overlapping pair of bins (say jj'-th) separated by a distance D in the phase space. The FCs are defined as [6, 7],

$$F'_{pq} = \frac{\langle n_j^{[p]}\, n_{j'}^{[q]}\rangle}{F'_p\, F'_q} \tag{3.22}$$

Table 3.8: Values of fit parameters of $\ln\langle F_2^{(2)}\rangle$ against $\ln M$ plot by using a quadratic function like $f(x) = ax^2 + bx + c$ for the ^{32}S-Ag/Br interaction. The errors are of statistical origin.

Hurst Exponent(H)	a	b	R^2
0.25	-0.0004±0.0019	0.0391±0.0135	0.887
0.30	0.0026±0.0018	0.0222±0.0129	0.915
0.35	-0.0014±0.0013	0.0507±0.0097	0.950
0.40	-0.00004±0.0011	0.0446±0.0085	0.968
0.50	0.0046±0.0009	0.0175±0.0081	0.981
0.60	0.0039±0.0007	0.0286±0.0063	0.991
0.70	0.0071±0.0008	0.0036±0.0078	0.989
0.80	0.0085±0.0007	-0.0067±0.0068	0.993
1.0	0.0136±0.0007	-0.0515±0.0083	0.994
1.08	0.0108±0.0007	-0.0234±0.0078	0.993
1.1	0.0107±0.0007	-0.0224±0.0070	0.994
1.2	0.0094±0.0007	-0.0117±0.0067	0.994
1.4	0.0080±0.0006	-0.0019±0.0061	0.994
1.5	0.0079±0.0006	-0.0011±0.0059	0.994
1.6	0.0065±0.0009	0.0108±0.0078	0.988
1.8	0.0056±0.0009	0.0138±0.0078	0.986
2.0	0.0081±0.0012	-0.0082±0.0098	0.976
2.5	0.0014±0.0011	0.0331±0.0084	0.967
3.0	0.0029±0.0016	0.0196±0.0115	0.934
4.0	0.0005±0.0018	0.0295±0.0123	0.888

where $n_j^{[q]} = n_j(n_j - 1)\cdots(n_j - q + 1)$ is the single event q-th order SFM, $F_q' = \langle n_j^{[q]}\rangle$ and n_j ($n_{j'}$) is the number of tracks in the j-th (j'-th) interval. The above defined FCs are not symmetric in the indices p and q, and therefore they are symmetrized as,

$$\langle F_{pq}\rangle = \frac{1}{2}\left(F'_{pq} + F'_{qp}\right) \tag{3.23}$$

According to the α-model of intermittency [6, 7] F_{pq} should depend on the correlation length D but not on the phase space interval size δX, and they should follow a power-law relation like,

$$\langle F_{pq}\rangle \propto D^{-\phi_{pq}} \tag{3.24}$$

as $1/D$ approaches a large value. The exponent ϕ_{pq} measures the strength of correlation. Figure 3.11 shows event averaged FCs as functions of correlation length in the η-space for the ^{16}O-Ag/Br interaction at 200A GeV/c. The experimental results are supplemented by the corresponding UrQMD and UrQMD+BEC generated results. For each combination of (p, q) the experimental values of $\langle F_{pq}\rangle$ increase with increasing $-\ln D$. It is seen that there is a rapidly growing correlation at the beginning, a saturation next, and a moderate linear rise at the end. On the other hand, with increasing $-\ln D$ the simulated values of $\langle F_{pq}\rangle$ rise initially and then saturate. Since the $-\ln D$ versus $\langle F_{pq}\rangle$ plots are not linear over the

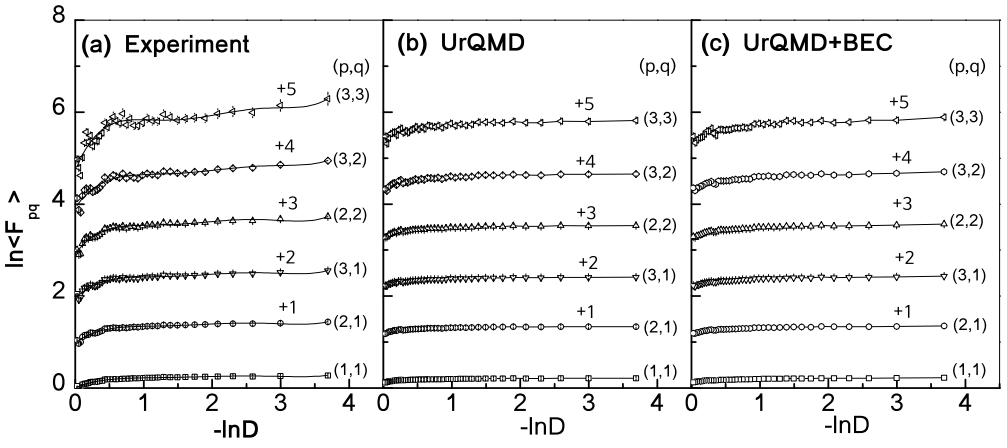

Figure 3.11: Plot showing the dependence of factorial correlators of different orders against correlation length for the ^{16}O-Ag/Br interaction at 200A GeV/c. Points represent (a) experimental values, (b)UrQMD values and (c)UrQMD+BEC values in η-space. For clarity correlators of successive orders are shifted by one unit along the vertical axis as shown in the diagram. Lines joining points are drawn to guide the eye.

entire range of $-\ln D$, the exponents ϕ_{pq} are obtained by fitting straight lines to the data only in the large $-\ln D$ region that corresponds to short-range correlations. The values of ϕ_{pq}, and the coefficient R^2, a measure of the goodness of fits, are given in Table 3.9 for the ^{16}O-Ag/Br interaction. For an easy reference we show the values for the ^{32}S-Ag/Br interaction in Table 3.10. Both experiments produce almost identical values of the exponent ϕ_{pq}. Negligibly small values of ϕ_{pq} are obtained from the UrQMD simulation. Inclusion of BEC only marginally enhances the values of the exponent in both interactions. According to the α-model and log-normal approximation ϕ_{pq} exponents should follow a relation like

$$\phi_{pq} = \phi_{p+q} - \phi_p - \phi_q = (p \cdot q)\,\phi_{11} \tag{3.25}$$

The validity of the above relation has been tested in Figure 3.12 by plotting ϕ_{pq} with the product $(p \cdot q)$ for both interactions. The results are consistent with a linear growth of the exponent ϕ_{pq} with the product $(p{\cdot}q)$, indicating the validity of the α-model in the ^{16}O-Ag/Br and ^{32}S-Ag/Br interactions at 200A GeV/c. UrQMD and UrQMD+BEC simulated results cannot match the respective experiment. The values of the slope parameter $\delta = \phi_{11}$ are given in Table 3.11. Another prediction of the α-model is that $\langle F_{pq}\rangle$ should be independent of δX_η. This aspect can be verified from Figure 3.13, where the values of $\langle F_{pq}\rangle$ obtained from the ^{16}O-Ag/Br data are plotted for several different values of δX_η at fixed D. Horizontal lines showing the uniformity of the $\langle F_{pq}\rangle$ distributions are drawn to guide the eye. Although a few points at large $-\ln \delta X_\eta$ and higher (p, q) slightly deviate from the average trend, in general considering the error bars, the prediction of the α-model is fulfilled in the ^{16}O-Ag/Br experiment. Similar results were also obtained for the ^{32}S-Ag/Br experiment [21]. It must

Table 3.9: The ϕ_{pq} exponents of the FC scaling for several different combinations of (p, q) for the ^{16}O-Ag/Br interaction.

	Experiment		UrQMD		UrQMD+BEC	
(p,q)	ϕ_{pq}	R^2	ϕ_{pq}	R^2	ϕ_{pq}	R^2
(1,1)	0.016±0.001	0.952	0.005±0.008	0.698	0.007±0.011	0.886
(2,1)	0.031±0.002	0.971	0.008±0.002	0.685	0.013±0.002	0.847
(3,1)	0.049±0.002	0.980	0.011±0.002	0.672	0.018±0.003	0.825
(2,2)	0.068±0.003	0.983	0.014±0.003	0.665	0.023±0.003	0.832
(3,2)	0.127±0.007	0.977	0.022±0.005	0.631	0.034±0.006	0.767
(3,3)	0.209±0.015	0.963	0.029±0.001	0.554	0.046±0.002	0.887

Table 3.10: The ϕ_{pq} exponents of the FC scaling for several different combinations of (p, q) for the ^{32}S-Ag/Br interaction.

	Experiment		UrQMD		UrQMD+BEC	
(p,q)	ϕ_{pq}	R^2	ϕ_{pq}	R^2	ϕ_{pq}	R^2
(1,1)	0.015±0.002	0.943	0.007±0.001	0.783	0.008±0.001	0.827
(2,1)	0.027±0.004	0.927	0.012±0.002	0.782	0.014±0.002	0.838
(3,1)	0.045±0.006	0.932	0.016±0.003	0.780	0.019±0.003	0.843
(2,2)	0.056±0.007	0.948	0.021±0.004	0.785	0.025±0.003	0.844
(3,2)	0.109±0.009	0.973	0.029±0.005	0.800	0.035±0.005	0.848
(3,3)	0.195±0.010	0.990	0.037±0.006	0.777	0.046±0.007	0.831

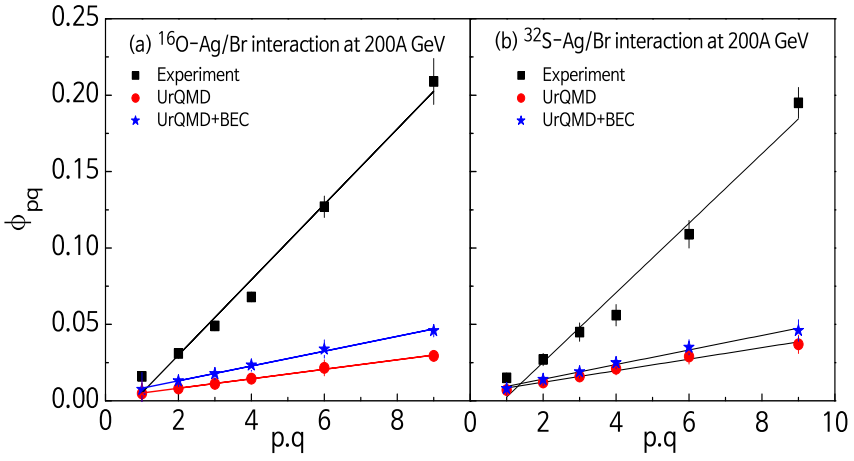

Figure 3.12: Plot of ϕ_{pq} versus $p.q$ in η-space according to the predictions of the α-model. The solid line is the best-fit straight line to the experimental values.

be mentioned that such a property does not only hold for the α-model, but it is in general a feature of any model that takes short-range correlations into account [94]. Our results on FCs indicate the presence of short-range bin-to-bin correlations in the experiment, and the gross features of the experiments are consistent with the prediction of the α-model. The correlation strength in the UrQMD generated data sample for each interaction is negligibly small, much smaller (almost by an order of magnitude) than the corresponding experiment.

Table 3.11: The values of slope parameter (δ) obtained from the ϕ_{pq} vs $(p \cdot q)$ plot.

	^{16}O-Ag/Br		^{32}S-Ag/Br	
	δ	R^2	δ	R^2
Experiment	0.025±0.001	0.994	0.023±0.002	0.988
UrQMD	0.003±0.0001	0.998	0.004±0.0002	0.992
UrQMD+BEC	0.005±0.0001	0.998	0.005±0.0002	0.995

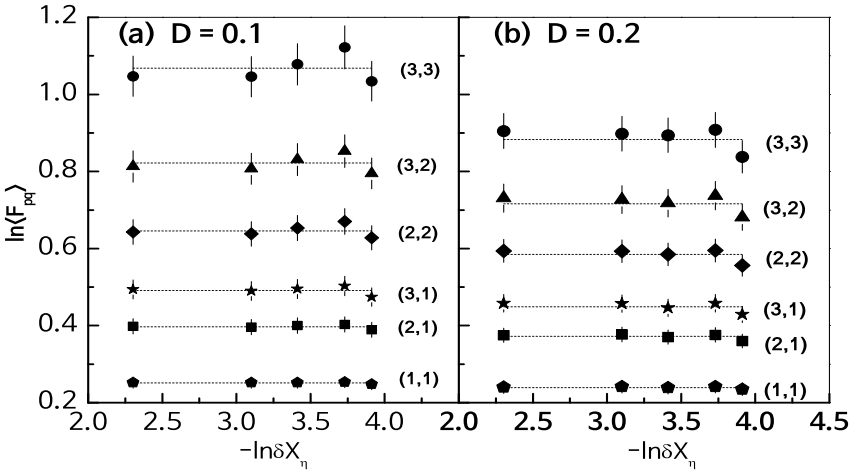

Figure 3.13: Plot showing independence of factorial correlators with respect to phase space partition size δX_η at fixed D for the ^{16}O-Ag/Br interaction at 200A GeV/c. The dotted lines are best fit straight lines to the data.

3.5 Oscillatory moments

The effect of multiparticle correlation can also be studied by using the factorial cumulant moments K_q [95]. They measure the genuine higher order correlations, where contributions from lower order correlations are eliminated. The K_q-moments are defined as,

$$K_q = F_q - \sum_{j=1}^{q-1} \binom{q-1}{j-1} F_{q-j} K_j \quad : \; q = 2, 3, \cdots \tag{3.26}$$

For Poisson distributed multiplicities $K_1 = 1$ and $K_{q>1} = 0$. Thus, nonzero values of K_q for $q \geq 2$, indicate the presence of two or more particle correlations in the inclusive density distribution of the produced particles. It has been predicted by a QCD-based parton shower cascade model that with increasing q the K_q moments would oscillate irregularly around zero. Both F_q and K_q possess strong energy and order dependence. In order to take care of such trivial dependences, a new set of normalized cumulant moments are defined [16] as,

$$H_q = K_q / F_q \tag{3.27}$$

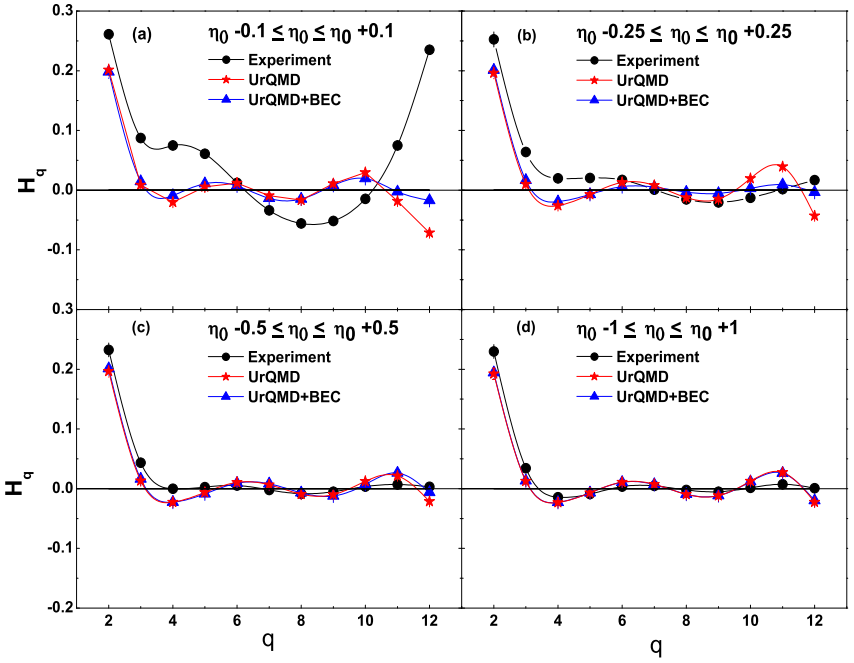

Figure 3.14: Oscillatory moments H_q for different widths of η interval. In each η interval, experiment, UrQMD and UrQMD+BEC results are plotted together. $H_q = 0$ is the horizontal solid line. The graph is for the ^{16}O-Ag/Br interaction at 200A GeV/c.

In high-energy e^+e^-, hadron-hadron (hh), and hadron-nucleus (hA) interactions, oscillatory behavior of the H_q-moments with increasing q has been experimentally confirmed [1–4, 17, 96]. For the e^+e^- and hh interactions the observed behavior has been attributed to a multicomponent structure of the particle production process, whereas for hA interactions the result has been explained in terms of a leading particle cascade model [97]. Empirically, a negative binomial distribution and/or a modified negative binomial distribution have/has been used to describe the multiplicity distributions in these interactions. But neither of them could explain the behavior of the cumulant moments [98]. The H_q moments computed for the ^{16}O-Ag/Br and ^{32}S-Ag/Br interactions at 200A GeV/c are shown in Figure 3.14 and Figure 3.15 respectively. In these figures the experimental results are compared with the UrQMD and UrQMD+BEC simulated results. The normalized oscillatory moments H_q are calculated in several different η-windows positioned symmetrically about the centroid (η_0) of the respective η-distribution like, (i) $\eta_0 - 0.1 \leq \eta_0 \leq \eta_0 + 0.1$, (ii) $\eta_0 - 0.25 \leq \eta_0 \leq \eta_0 + 0.25$, (iii) $\eta_0 - 0.5 \leq \eta_0 \leq \eta_0 + 0.5$ and (iv) $\eta_0 - 1.0 \leq \eta_0 \leq \eta_0 + 1.0$. One can see that only in the narrowest η-window the experimental results are significantly different from the UrQMD and UrQMD+BEC results. The extent of oscillation, particularly at large q, is much larger for the experiment than what it is either for the UrQMD or the UrQMD+BEC data. This is indicative of different characteristics of the jet structure in the experiment and simulation. At small q the oscillation starts even before H_q drops down to zero. The UrQMD and UrQMD+BEC data on the other hand, exhibit smaller amplitudes of oscillation

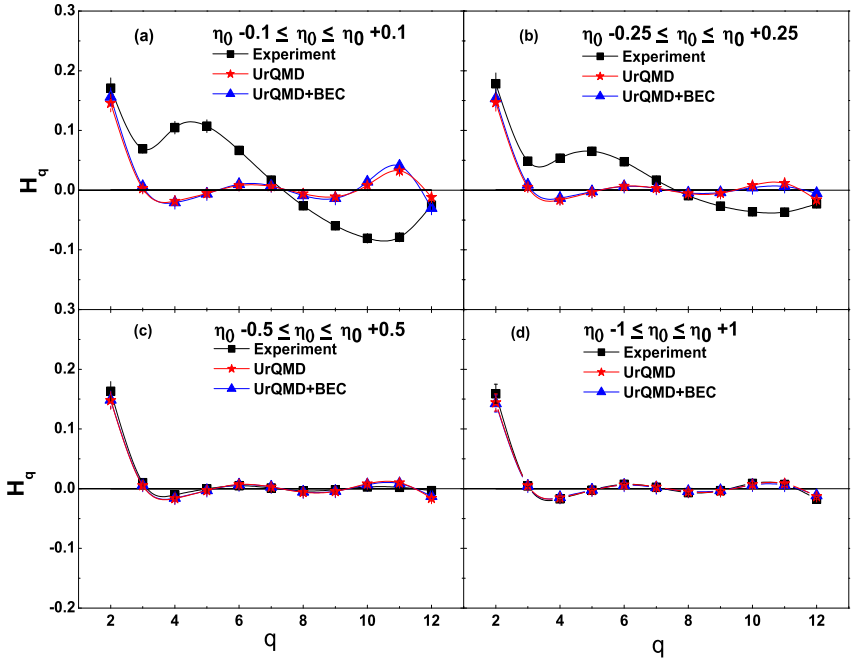

Figure 3.15: The same as in Figure 3.14 but for the ^{32}S-Ag/Br interaction at 200A GeV/c.

compared to the respective experiment. As the η-interval size increases, the difference between experiment and simulation tends to decrease. In large η-windows, particularly in $\eta_0 \pm 0.5$ and $\eta_0 \pm 1.0$, perhaps due to intermixing of particles coming from different sources, the correlation effects are washed out. The moments therefore show only very little or no oscillation, and the experimental results begin to coincide with the simulations. The above observations are more or less identical for both ^{16}O-Ag/Br and ^{32}S-Ag/Br interactions at 200A GeV/c.

3.6 Erraticity moments

As mentioned above the erraticity moments deal with the event space fluctuations of the factorial moments. We define a single event factorial moment F_q^e of order q as,

$$F_q^e = \frac{\frac{1}{M}\sum_{m=1}^{M} n_m(n_m-1)....(n_m-q+1)}{(\frac{1}{M}\sum_{m=1}^{M} n_m)^q} \tag{3.28}$$

M is the number of non-overlapping intervals in the η-space and n_m is the number of particles in the m-th such interval. Figure 3.16 shows the distributions of F_q^e for the ^{16}O-Ag/Br interaction for $M = 5$ and $M = 10$. The experimental results are compared with the corresponding UrQMD and UrQMD+BEC simulated events. It can be seen that majority of the F_q^e values are concentrated within an initial small range. However, a long, slowly decaying

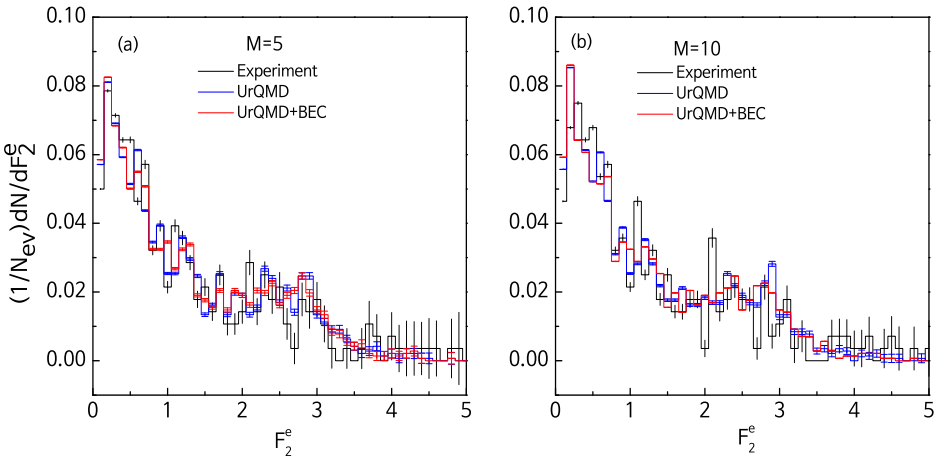

Figure 3.16: Distributions of F_2^e in the ^{16}O-Ag/Br interaction at 200A GeV/c for two different values of η space partition number (a) $M = 5$ and (b) $M = 10$.

tail that corresponds to growingly larger F_q^e values, is also visible in each distribution. It is our objective to quantify these large fluctuations in F_q^e in terms of the erraticity moments and associated parameters.

The method of erraticity analysis starts by introducing an event-wise normalized factorial moment $\Phi_q = F_q^e/\langle F_q^e \rangle$, and then by defining a couple of erraticity moments expressed in terms of Φ_q. The vertically averaged p-th order moment of Φ_q or the erraticity moment is defined as,

$$C_{p,q} = \langle \Phi_q^p \rangle \tag{3.29}$$

and an entropy like quantity Σ_q is defined as,

$$\Sigma_q = \langle \Phi_q \ln \Phi_q \rangle \tag{3.30}$$

In the $p > 1$ region $C_{p,q}$ characterizes the tails of F_q^e-distribution and is sensitive only to the spikes of the corresponding η-distribution. On the other hand $C_{p<1,\,q}$ characterizes the small F_q^e behavior of the F_q^e-distribution, which is influenced mainly by η-bins with low multiplicities. A typical domain of analysis is $0 < p < 2$, which reveals enough information about the F_q^e-distribution. We are particularly interested in studying the erraticity behavior in the $p \approx 1$ region. In multiparticle dynamics the erraticity moments $C_{p,q}$ are found to follow a scaling-law with phase space partition number M (equivalently with the window size $\delta\eta$) like,

$$C_{p,q} \propto M^{\psi(p,q)} \quad : \quad M \to \infty \tag{3.31}$$

The above equation is referred to as *the erraticity*, and the exponent $\psi(p,q)$ is called *the erraticity index*. If the spatial pattern of particle density function does not change from

one event to another, the distribution $P(F_q^e)$ tends to a delta function. Under such circumstances, both ϕ_q and $C_{p,q}$ would reduce to unity and $\psi(p,q) \to 0$. Any deviation of $\psi(p,q)$ from zero value can therefore be considered as an erraticity measure. The slope parameter,

$$\mu_q = \frac{d}{dp}\,\psi_q(p)\mid_{p=1} \tag{3.32}$$

is called the entropy index. In high-energy AB interactions $C_{p,q}$ may not exhibit as strict a scaling-law as prescribed in Equation (3.31), but would rather abide by a more generalized formula like,

$$C_{p,q} \propto f(M)^{\tilde{\psi}(p,q)} \tag{3.33}$$

where $f(M)$ is some well behaved function of M. Similar to Equation (3.33) one would expect a generalized scaling-law for the Σ_q moments like,

$$\Sigma_q \propto \tilde{\mu}_q\, \ln[f(M)] \tag{3.34}$$

From Equation (3.33) and Equation (3.34) it follows that

$$\tilde{\mu}_q = \frac{d}{dp}\tilde{\psi}(p,q)|_{p=1} \tag{3.35}$$

The index $\tilde{\mu}_q$ is quite different from the entropy index μ_q, and therefore, should not be compared with each other. However, the exponent $\tilde{\mu}_q$ is again a measure of the erratic behavior of the event space fluctuation of the factorial moments [19, 20]. A small $\tilde{\mu}_q$ value corresponds to a less chaotic system, whereas a large $\tilde{\mu}_q$ value corresponds to a highly chaotic system.

In Figure (3.17) the $C_{p,q}$ moments for $q = 2$ and 3 over a wide range of p-values are plotted against M for the ^{16}O-Ag/Br interaction. For a better comparison the experiment and simulation are plotted together. From these graphs one can see that the experimental $C_{p,q}$ values vary over a wider range compared to the corresponding UrQMD and UrQMD+BEC generated values. A smooth but nonlinear increasing trend of $\ln C_{p,q}$ with $\ln M$ can be seen over its entire range, which indicates the justification of invoking a generalized power-law as prescribed in Equation (3.33). Several kinks (or discontinuities) seen at large M for all the plots might be an outcome of the limited statistics of our event sample(s). A similar pattern is also observed for the ^{32}S-Ag/Br interaction at 200A GeV/c. To establish a generalized scaling-law as suggested by Cao and Hwa [19, 20], we have assumed $\ln f(M) = (\ln M)^b$, taking b as a free parameter that may be adjusted from the linear fit of the $\ln C_{2,2}$ versus $\ln[f(M)]$ data. Such plots are shown in Figure 3.18 along with the respective best fitted straight lines. The values of b so obtained, are given in the third column of Table 3.12. In all the cases Pearson's coefficient R^2, which decides the goodness of fit, are found to be > 0.98.

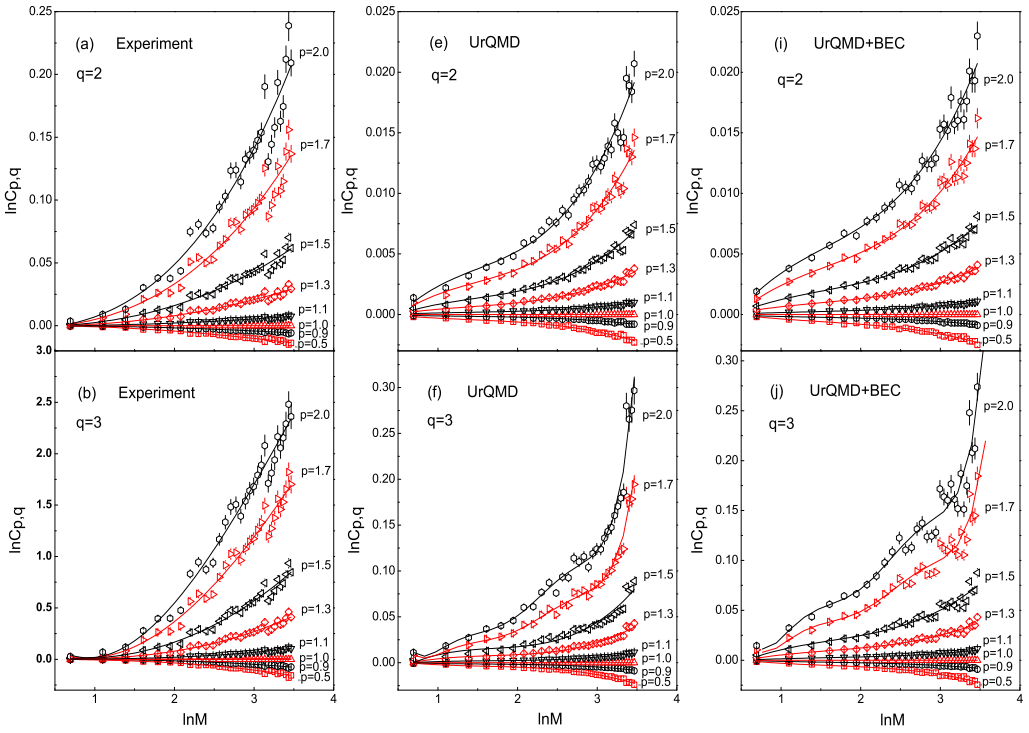

Figure 3.17: Erraticity moments $C_{p,q}$ plotted as functions of phase space partition number M for the ^{16}O-Ag/Br interaction. The solid curves are drawn to guide the eye.

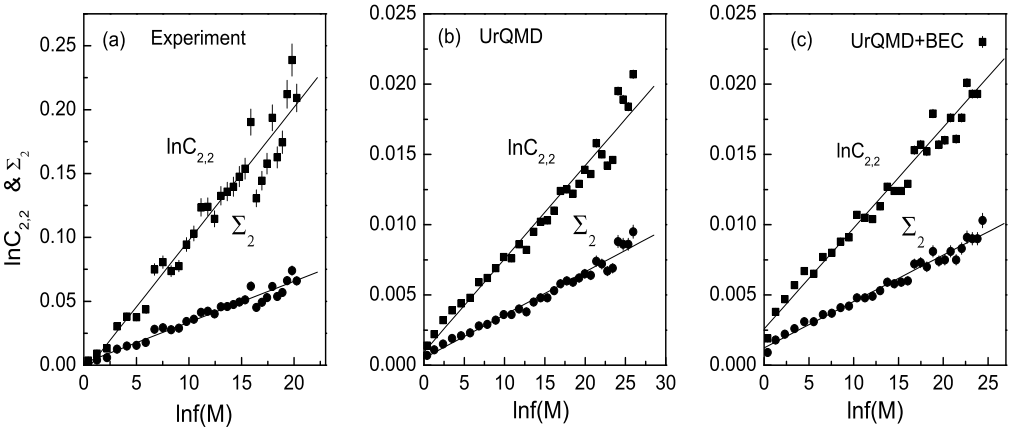

Figure 3.18: Plot of $\ln C_{2,2}$ and Σ_2 with $\ln f(M) = \ln M^b$ for the ^{16}O-Ag/Br interaction. The lines represent best linear fits to the data points.

The slope of the $\ln[f(M)]$ versus $\ln C_{2,2}$ straight line fit gives us another parameter ($\tilde{\psi}(2,2)$) related to the erraticity analysis. The $\tilde{\psi}(2,2)$ values are quoted in the fourth column of Table 3.12. The indices $\tilde{\mu}_2$ can now be obtained from the linear relationship between Σ_2 and $\ln[f(M)]$ using the b-values already obtained from the best fit. These plots are also included in Figure 3.18 and $\tilde{\mu}_2$ values are given in the fifth column of Table 3.12. Note that all the $C_{p,q}$ moments depend almost similarly on $\ln M$. In order to evaluate the erraticity

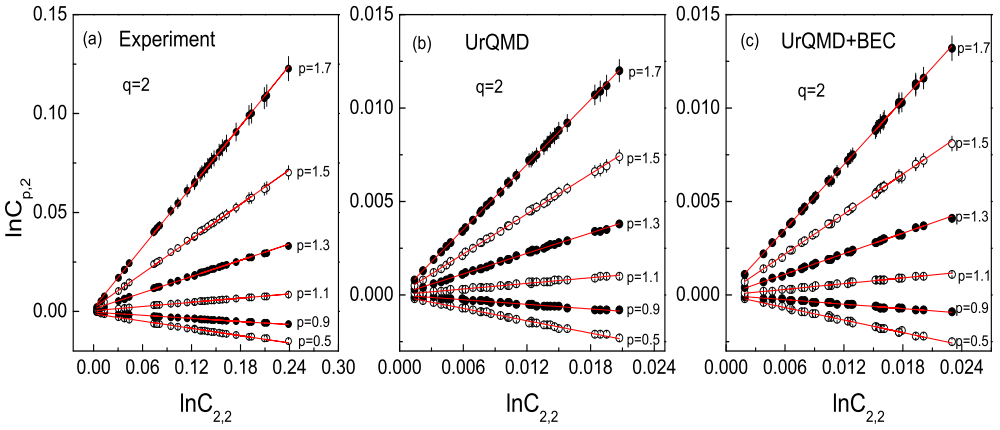

Figure 3.19: Plot of $\ln C_{p,2}$ with $\ln C_{2,2}$ for the ^{16}O-Ag/Br interaction. The best fitted straight lines are shown.

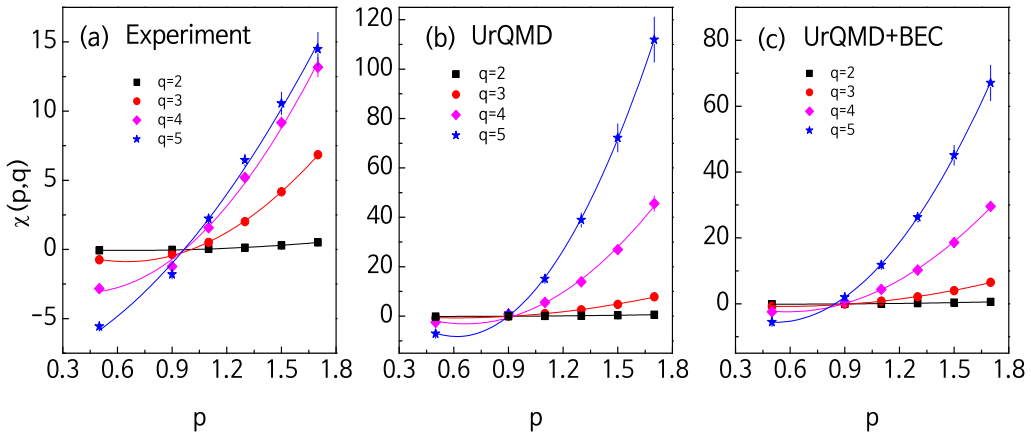

Figure 3.20: Variation of $\chi(p,q)$ with p for the ^{16}O-Ag/Br interaction. The curves represent the best quadratic fits.

parameters, one can therefore also use $\ln C_{2,2}$ in place of $\ln[f(M)]$. The scaling relation (Equation 3.33) then would reduce to a simple power law like,

$$C_{p,q} \propto (C_{2,2})^{\chi(p,q)} \tag{3.36}$$

We find that for $q = 2$ the expected linear dependence of $\ln C_{p,q}$ on $\ln C_{2,2}$ is almost exact. For different values of p the results are graphically presented in Figure 3.19 for the ^{16}O-Ag/Br interaction. For $q > 2$ the linear dependence is only approximate in the sense that it is valid only in the low-M region. The effects of finite multiplicity and limited statistics are visible at large M. For $q > 2$ we have obtained $\chi(p,q)$ through a linear fit of the $\ln C_{p,q}$ versus $\ln C_{2,2}$ data within a limited region of M (≤ 12), where $\ln C_{p,q}$ is found to behave systematically with $\ln C_{2,2}$. Figure 3.20 shows the $\chi(p,q)$ versus p plots for different q values for the ^{16}O-Ag/Br interaction. The solid lines in these diagrams represent a quadratic

Table 3.12: Values of b, $\tilde{\psi}(2,2)$ & $\tilde{\mu}_2$ for the experiment, the UrQMD and the UrQMD+BEC data.

Interaction	Data Set	b	$\tilde{\psi}(2,2)$	$\tilde{\mu}_2$
^{16}O-Ag/Br interaction	Experiment	2.42	0.0104±0.0005	0.0032±0.0001
at 200A GeV/c	UrQMD	2.62	0.0007±0.00002	0.0003±0.00009
	UrQMD+BEC	2.57	0.0007±0.00009	0.00033±0.00002
^{32}S-Ag/Br interaction	Experiment	2.08	0.0029±0.00007	0.00126±0.00003
at 200A GeV/c	UrQMD	2.52	0.00011±0.000003	0.00006±0.0000021
	UrQMD+BEC	2.22	0.0002±0.000007	0.00009±0.000004

function for a fixed q like,

$$\chi(p,q) = a_2\, p^2 + a_1\, p + a_0 \tag{3.37}$$

The first order derivatives of $\chi(p,q)$ at $p = 1$

$$\chi_q^{'} = \frac{\partial}{\partial p}\chi(p,q)|_{p=1} \tag{3.38}$$

can now be used to determine the $\tilde{\mu}_q$ index from the following relation,

$$\tilde{\mu}_q = \tilde{\psi}(2,2)\chi_q^{'} \tag{3.39}$$

In Figure 3.21 the entropy-like moments Σ_q are also plotted against $\ln M$ for different q-values. As expected, these moments are also nonlinear functions of $\ln M$. However, for all positive q the variations look quite similar. This gives us a freedom to use Σ_2 as the independent variable in place of $f(M)$. The plots of Σ_q against Σ_2 are shown in Figure 3.22 for our ^{16}O-Ag/Br data and corresponding simulations. In each case the slope parameters

$$\omega_q = \frac{\partial\, \Sigma_q}{\partial\, \Sigma_2} \tag{3.40}$$

are obtained by making a linear fit of the Σ_q versus Σ_2 plots within a limited $M\,(\leq 12)$ region. Subsequently, once again we derive the $\tilde{\mu}_q$ index by using the following relation,

$$\tilde{\mu}_q = \tilde{\mu}_2\, \omega_q \tag{3.41}$$

All four erraticity parameters namely $\chi_q^{'}$, ω_q and two sets of $\tilde{\mu}_q$ obtained from Equation (3.39) and Equation (3.41), have been presented in Table 3.13 for the ^{16}O-Ag/Br interaction at 200A GeV/c. Table 3.14 on the other hand shows the corresponding values for the ^{32}S-Ag/Br interaction. The parameters obtained from the experiment as well as from the simulations are presented together for an easy comparison. Several observations can now be

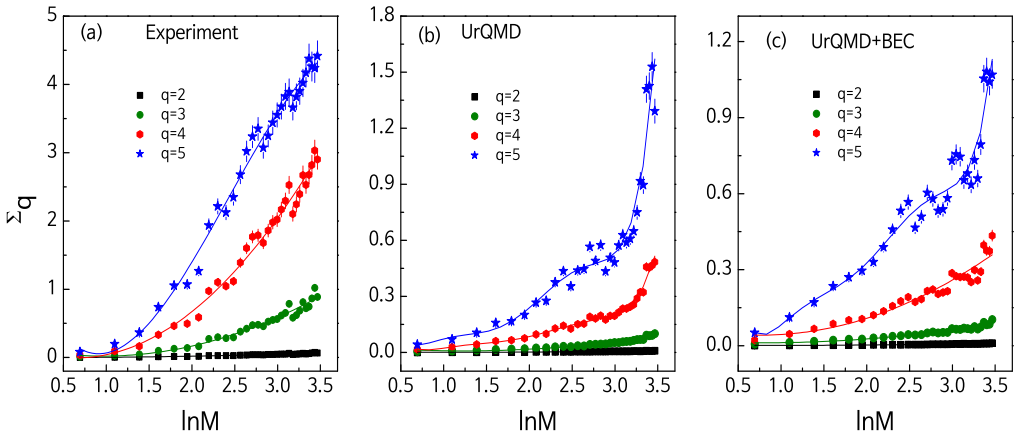

Figure 3.21: Plot of Σ_q with $\ln M$ for the ^{16}O-Ag/Br interaction. The lines joining points are drawn to guide the eye.

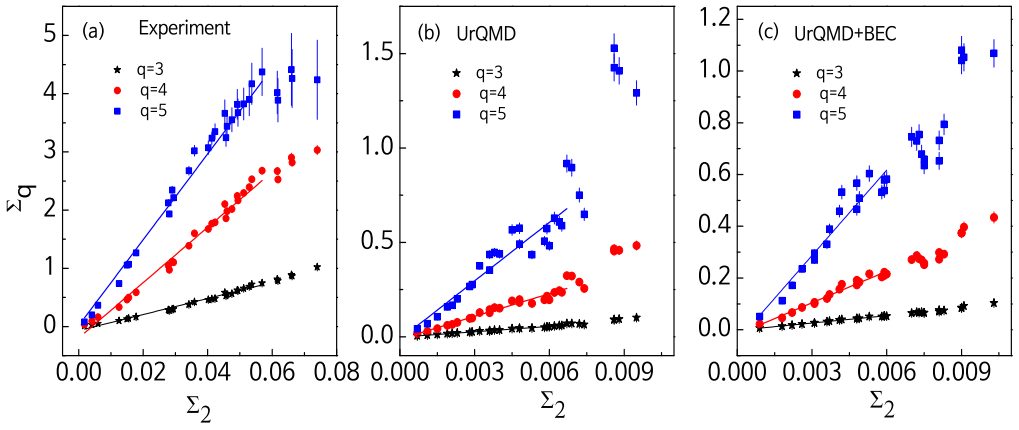

Figure 3.22: Plot of Σ_q against Σ_2 for the ^{16}O-Ag/Br interaction. The lines represent best linear fits to the data points in the $M \leq 12$ region.

made regarding the erraticity behavior of the interactions studied in this analysis. In general, erraticity in the particle production mechanism is observed for all the data sets used. The index $\tilde{\mu}_q$ obtained by using two different formulae, Equation (3.39) and Equation (3.41), within their statistical uncertainties, are very close to each other for both the interactions under consideration. In the ^{16}O-Ag/Br experiment the $\tilde{\mu}_q$ values are greater than the corresponding ^{32}S-Ag/Br values. For a better understanding $\tilde{\mu}_q$ values are plotted with q in Figure 3.23 for the ^{16}O-Ag/Br data. Figure 3.23(a) is drawn following Equation (3.39) and Figure 3.23(b) following Equation (3.41). In these diagrams the experimental $\tilde{\mu}_q$ values show a rapid growth with increasing q and the values are always larger than the corresponding simulated values. Almost an identical pattern was observed also for the ^{32}S-Ag/Br interaction at 200A GeV/c [23]. For the ^{28}Si-Ag/Br interaction at 14.5A GeV [79] the exponent values are found to be slightly less than that obtained either in the ^{16}O-Ag/Br or in the ^{32}S-Ag/Br interaction at 200A GeV/c. Comparing the results of our erraticity analysis with

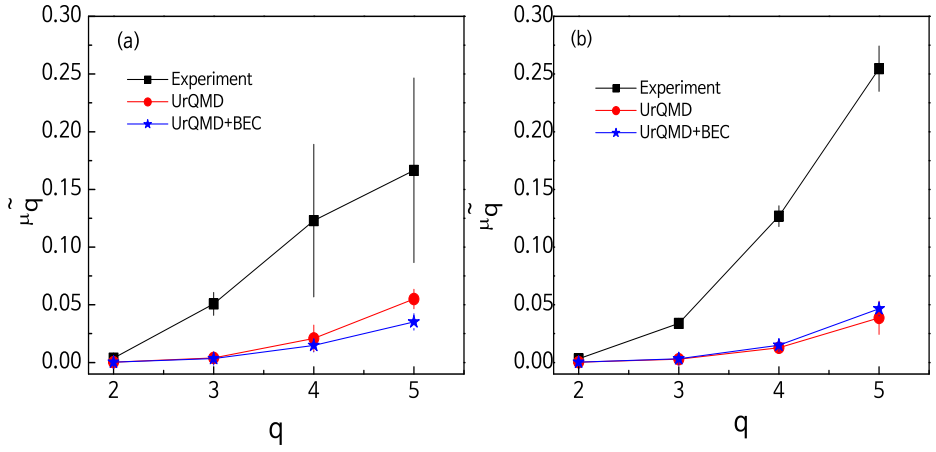

Figure 3.23: Plot of the entropy index $\tilde{\mu}_q$ against order number q calculated from (a) Equation (3.39) and (b) Equation (3.41) for the ^{16}O-Ag/Br interaction. Lines joining the data points are shown.

similar results available in literature[68, 79], one can argue that the parameters depend more on the colliding system (projectile mass number) than on the energy of the collision. An increase in the entropy index signals the augmentation of a possible quark-hadron phase transition [99]. This feature has indeed been observed for a possible non-thermal phase transition [100]. We find a similar increasing trend in the $\tilde{\mu}_q$ parameter for the present set of ^{16}O-Ag/Br and ^{32}S-Ag/Br data, that might be a signal of non-thermal phase transition. For all the parameters studied in connection with our erraticity analysis the UrQMD and UrQMD+BEC simulated results cannot match the respective experiment. It looks like that

Table 3.13: Erraticity parameters in the ^{16}O-Ag/Br interaction at 200A GeV/c.

Order	$\chi_q^{'}$	ω_q	$\tilde{\mu}_q = \tilde{\psi}(2,2)\,\chi_q^{'}$	$\tilde{\mu}_q = \tilde{\mu}_2\,\omega_q$
		-Experiment-		
2	0.3585±0.1526	–	0.0037±0.0018	0.0032±0.0001
3	4.8897±0.7076	10.5999±0.2905	0.0509±0.0099	0.0339±0.0020
4	11.8182±5.7735	39.5938±1.4085	0.1231±0.0661	0.1268±0.0090
5	16.0123±7.7193	79.5720±2.8979	0.1668±0.0880	0.2546±0.0197
		-UrQMD-		
2	0.4691±0.0358	–	0.0003±0.00003	0.0003±0.0001
3	5.5574±2.0006	9.4482±0.2546	0.0039±0.0015	0.0028±0.0009
4	29.9204±15.4343	42.3925±2.0933	0.0209±0.0114	0.0127±0.0044
5	78.5247±9.8705	129.1417±9.5503	0.0549±0.0085	0.0387±0.0145
		-UrQMD+BEC-		
2	0.4704±0.0415	–	0.0003±0.0001	0.0003±0.00002
3	4.8484±1.0341	9.9323±0.2553	0.0034±0.0012	0.0033±0.0003
4	21.1468±4.8363	45.5489±2.3834	0.0148±0.0053	0.0150 ±0.0017
5	50.2871±3.7539	140.9617±10.0848	0.0352±0.0072	0.0465±0.0062

Table 3.14: Erraticity parameters in the ^{32}S-Ag/Br interaction at 200A GeV/c.

Order	$\chi_q^{'}$	ω_q	$\tilde{\mu}_q = \tilde{\psi}(2,2)\,\chi_q^{'}$	$\tilde{\mu}_q = \tilde{\mu}_2\,\omega_q$
		-Experiment-		
2	0.4370±0.0540	–	0.0013±0.0002	0.0013±0.00003
3	7.0600±1.7400	15.550±0.5400	0.0210±0.0050	0.0195±0.0008
4	33.980±3.1700	79.630±3.3300	0.0990±0.0090	0.1000±0.0050
5	72.260±17.370	191.20±4.9900	0.2100±0.0500	0.2400±0.0080
		-UrQMD-		
2	0.4970±0.0760	–	0.0001±0.00001	0.0001±0.000002
3	4.2910±0.1640	8.4090±0.1630	0.0005±0.00003	0.0005±0.00003
4	18.6530±1.5790	35.987±1.1390	0.0021±0.0002	0.0022±0.0001
5	57.907±9.7320	108.523±4.8190	0.0064±0.0012	0.0065±0.0005
		-UrQMD+BEC-		
2	0.4910±0.0600	–	0.0001±0.00002	0.0001±0.000004
3	4.9360±0.4970	9.7120±0.2480	0.0009±0.0001	0.0009±0.00006
4	26.4630±9.7890	47.5750±2.2710	0.0053±0.0021	0.0043±0.0004
5	104.978±65.882	167.643±12.791	0.0210±0.0139	0.0151 ±0.0018

the erraticity behavior comes merely as a statistical effect in the UrQMD model. Inclusion of BEC does not add any significant change in the observations.

3.7 Summary

In this chapter we have presented the results of our intermittency analysis and related issues on the shower track distribution in ^{16}O-Ag/Br interaction at 200A GeV/c. On many occasions our ^{16}O-Ag/Br results are compared with similar results obtained from the ^{32}S-Ag/Br interaction at 200A GeV/c. We also provide a systematic comparison of the experimental results with the predictions of the UrQMD and UrQMD+BEC models. Major observations of this analysis are summarized below.

(i) We find an intermittent pattern of the density distribution of the shower tracks in the ^{16}O-Ag/Br interaction at 200A GeV/c which is self-similar in the η or φ, and self-affine in (η, φ) space. The intermittency observed in ^{16}O-Ag/Br data is stronger than that observed in the ^{32}S-Ag/Br data. Comparing the results of this analysis with similar results available in the literature, we understand that the 1d intermittency depends more on the colliding objects than on the collision energy. Higher order particle correlations in ^{16}O-Ag/Br interaction cannot be fully explained in terms of two and three-particle (lower order) correlations. Since the shower tracks consist of both positive and negative charged mesons, not strictly identical fields, the observed

correlations are not exactly Bose-Einstein type either. The order dependence of the intermittency indexes rule out the possibility of a second-order thermal phase transition in the ^{16}O-Ag/Br and ^{32}S-Ag/Br interactions. However, a weak sign of a multiplicative cascade mechanism is observed in the experiments. The multifractal specific heat C has been calculated from the generalized Rényi dimensions. However, the values of C do not match with the universal expected value ($C = 0.25$) of the parameter.

(*ii*) Our analysis on factorial correlators indicate that short range bin-to-bin correlations are present in the data, and the experimental observations in this regard are consistent with the α-model. Once again the observed correlations could not be reproduced either by the UrQMD or by the UrQMD+BEC. The oscillatory moments are found to be quite sensitive to the type of correlations present in the experiment as well as in the simulations. The results on FCs and OMs therefore, cannot be simply interpreted in terms of a few particle correlations.

(*iii*) The $2d$ intermittency strength is significantly higher compared to that in the $1d$, i.e. dimensional reduction of underlying space affects the intermittency phenomenon. As expected, the UrQMD simulated results show almost negligible intermittency for both ^{16}O-Ag/Br and ^{32}S-Ag/Br interactions at 200A GeV/c. However, a small amount of intermittency is observed when the BEC is incorporated into the UrQMD output. The experimental values of $2d$ intermittency index $\phi_q^{(2)}$ are several times larger than the UrQMD+BEC simulated values. The $2d$ intermittency results suggest that the underlying fractal structure of the dynamical fluctuation is not self-similar at all scales, rather it is self-affine. The self-similarity could be retrieved only when the anisotropy in the (η, φ) plane is properly addressed by using the Hurst exponent H. In this analysis we find that the anisotropy in the $2d$ space can be retrieved for two different values of H, with $H = 0.4$ and $H = 4.0$. We do not attribute any physical significance to the value $H > 1.0$. However, for $H \sim 0.4$ the data behave in a more systematic and consistent manner. The fluctuation strength in $2d$ are always greater in the ^{16}O-Ag/Br interaction than in the ^{32}S-Ag/Br interaction.

(*iv*) A substantial amount of event-to-event fluctuations of the SFMs is observed in the ^{16}O-Ag/Br interaction at 200A GeV/c. The fluctuations are characterized by a power-law type of scaling of the erraticity moments $C_{p,q}$ and Σ_q against the partition number M. The event space fluctuations of the SFMs is found to be more chaotic in the ^{32}S-Ag/Br than in the ^{16}O-Ag/Br interaction. The UrQMD and UrQMD+BEC generated values of the SFM in both ^{16}O-Ag/Br and ^{32}S-Ag/Br interactions exhibit erraticity too. The chaoticity present in the UrQMD simulations are however not as prominent as they are in the experiments. A comparison of our results with those obtained from the transport model, as well as with the results obtained from other experiments on

hN, NN and AB interactions [20, 58, 59, 69] shows that, the chaoticity is significantly weaker in the present case than that obtained in other investigations.

Bibliography

[1] W. Kittel and E. A. De Wolf, Soft Multihadron Dynamics, World Scientific (2005).

[2] W. Kittel, Proceedings of the Twentieth International Symposium on Multiparticle Dynamics, Gut Holmeche, Germany (1990), Edited by R. Baier and D. Wegener, World Scientific, Singapore (1991).

[3] I. M. Dremin and J. W. Gary, Phys. Rep. 349, 301 (2001).

[4] E. A. De Wolf, I. M. Dremin and W. Kittel, Phys. Rep. 270, 1 (1996).

[5] Fluctuations and fractal structure, Proceedings of Ringburg Workshop on multiparticle production, Ringberg Castle, Germany, 1991, Edited by R. C. Hwa, W. Ochs and N. Schmitz, World Scientific, Singapore (1992).

[6] A. Bialas and R. Peschanski, Nucl. Phys. B 273, 703 (1986).

[7] A. Bialas and R. Peschanski Nucl. Phys. B 308, 857 (1988).

[8] T. H. Burnett *et al.*, Phys. Rev. Lett. 50, 2062 (1983).

[9] I. M. Dremin, Sov. J. Nucl. Phys. 30, 726 (1981).

[10] W. Ochs, Phys. Lett. B 247, 101 (1990).

[11] A. Bialas and K. Zalewski, Phys. Lett. B 238, 413 (1990).

[12] R. C. Hwa, Phys. Lett. B 201, 165 (1988).

[13] I. M. Dremin, JETP Lett. 30, 152 (1980).

[14] B. Andersson, P. Dahlquist and G. Gustafson, Phys. Lett. B 214, 604 (1988).

[15] B. C. Chiu and R. C. Hwa, Phys. Lett. B 236, 466 (1990).

[16] I. M. Dremin, Phys. Lett. B 313, 209 (1993).

[17] I. M. Dremin *et al.*, Phys. Lett. B 336, 119 (1994).

[18] Z. Cao and R. C. Hwa, Phys. Rev. Lett. 75, 1268 (1995).

[19] Z. Cao and R. C. Hwa, Phys. Rev. D 53, 6608 (1996).

[20] Z. Cao and R. C. Hwa, Phys. Rev. D 61, 074011 (2000).

[21] M. K. Ghosh, A. Mukhopadhyay and G. Singh, J. Phys. G 34, 177 (2007).

[22] D. Chanda, M. K. Ghosh *et al.*, Phys. Rev. C 71, 034904 (2005).

[23] M. K. Ghosh and A. Mukhopadhyay, Phys. Rev. C 68, 034907 (2003).

[24] R. Holynski *et al.*, Phys. Rev. Lett. 62, 733 (1989).

[25] A. Bialas and R. Peschanski, Jagellonian University Report No. TPJU/4/88.

[26] R. Holynski *et al.* (KLM Collaboration), Phys. Rev. C 40, R2449 (1989).

[27] M. I. Adamovich *et al.*, Phys. Rev. Lett. 65, 412 (1990).

[28] P. L. Jain *et al.*, Phys. Rev. Lett. 59, 2531 (1987).

[29] G. Singh *et al.*, Phys. Rev. Lett. 61, 1073 (1988).

[30] K. Sengupta *et al.*, Phys. Lett. B 213, 548 (1988).

[31] P. L. Jain *et al.*, Phys. Lett. B 187, 175 (1987); Phys. Rev. D 34, 2886 (1986).

[32] K. Sengupta *et al.*, Phys. Lett. B 236, 219 (1990).

[33] G. Singh, A. Mukhopadhyay and P. L. Jain, Z. Phys. A 345, 305 (1993).

[34] P. L. Jain and G. Singh, Phys. Rev. C 44, 854 (1991).

[35] P. L. Jain and G. Singh Z. Phys. C 53, 355 (1992).

[36] G. Das *et al.*, Phys. Rev. C 54, 2081 (1996).

[37] D. Ghosh *et al.*, Phys. Rev. C 47, 1120 (1993).

[38] P. L. Jain and G. Singh, Nucl. Phys. A 596, 700 (1996).

[39] P. Mali, A. Mukhopadhyay and G. Singh, Phys. Scr. 85, 065202 (2012).

[40] M. Mohisin Khan *et al.*, Int. J. Mod. Phys. E 23, 1450075 (2014).

[41] I. V. Ajinenko *et al.*, Phys. Lett. B 222, 306 (1989).

[42] A. Capella *et al.*, Phys Lett. B 81, 68 (1979); Z. Phys. C 3, 329 (1980).

[43] M. Adamus *et al.*, (NA22 Collaboration), Z. Phys. C 39, 311 (1988).

[44] B. Buschbeck *et al.*, Phys. Lett. B 215, 788 (1988).

[45] R. Peschanski, Proc. 23èmes Rencontres de Moriond (Les Arcs, Savoie, March 1988), ed. Tran Thanh Van Editions Frontières, Gif-sur-Yvette) (1988).

[46] T. Haupt (NA22 Collaboration), Proc. XIX Intern. Symp. on Multiparticle dynamics (1988), ed. Tran Thanh Van (Editions Frontières, Gif-sur-Yvette) (1988).

[47] C. Albajar *et al.* (UA1 Collaboration), Nucl. Phys. B 345, 1 (1990).

[48] P. Abreu *et al.* (DELPHI Collaboration), Phys. Lett. B 247, 137 (1990).

[49] T. Sjöstrand, Comput. Phys. Commun. 27, 243 (1982); Comput. Phys. Commun. 28, 229 (1983); T. Sjöstrand and M. Bengtsson, Comput. Phys. Commun. 43, 367 (1987).

[50] W. Braunschweig *et al.* (TASSO Collaboration), Phys. Lett. B 231, 548 (1989).

[51] K. Sugano, (HRS Collaboration), Contribution to the Workshop on Interrnittency in high energy collisions, Santa Fe, March (1990).

[52] G . Gustafson and C. Sjögren, Phys. Lett. B 248, 430 (1990).

[53] N. M. Agababyan *et al.* (EHS /NA22 Collaboration), Phys. Lett. B 382, 305 (1996).

[54] S. Wang *et al.*, Phys. Lett. B 458, 505 (1999).

[55] F. Jinghua *et al.*, Phys. Lett. B 472, 161 (2000).

[56] L. Fuming *et al.*, Phys. Lett. B 516, 293 (2001).

[57] Yi-Fei Zhou *et al.*, Chin. Phys. Lett. 18, 1179 (2001).

[58] W. Shaoshun and W. Zhaomin Phys. Rev. D 57, 3036 (1998).

[59] D. Ghosh *et al.*, Phys. Lett. B 540, 52 (2002).

[60] D. Ghosh *et al.*, J. Phys. G 29, 2087 (2003).

[61] Z. Cao and R. C. Hwa, Phys. Rev. D 54, 6674 (1996).

[62] L. Zhixu, F. Jinghua and L. Lianshou, HZPP-9909, July 30 (1999).

[63] I. V. Ajineko *et al.* (NA22 Collaboration), Phys. Lett. B 235, 373 (1990).

[64] M. R. Atayan *et al.* (EHS/NA22 Collaboration), Phys. Lett. B 558, 29 (2003).

[65] T. Sjöstrand, Comput. Phys. Commun. 82, 74 (1994).

[66] M. R. Atayan *et al.*, (EHS/NA22 Collaboration), Phys. Lett. B 558, 22 (2003).

[67] R. Hasan *et al.*, J. Phys. G 28, 2939 (2002).

[68] S. Ahmad *et al.*, J. Phys. G 30, 1145 (2004).

[69] M. R. Atayan *et al.*, (EHS/NA22 Collaboration), HEN 449 (2003).

[70] D. Ghosh *et al.*, J. Phys. G 34, 2165 (2007).

[71] D. Ghosh *et al.*, J Phys. G 31, 1083 (2005).

[72] D. Ghosh *et al.*, Phys. Rev. C 68, 024908 (2003).

[73] R. Botet and M. Ploszajczak, The Phenomenology of Hadronic Matter, World Scientific Lecture Notes in Physics Vol. 65, World Scientific (2002).

[74] A. Bialas and M. Gazdzicki, Phys. Lett. B 252, 483 (1990).

[75] M. I. Adamovich *et al.* (EMU01 Collaboration), Z. Phys. C 76, 659 (1997).

[76] M. I. Adamovich *et al.* (EMU01 Collaboration), Nucl. Phys. B 388, 3 (1992).

[77] H. Pi, Comp. Phys. Commun. 71, 173 (1992).

[78] P. R. Bevington and D. K. Robinson, Data reduction and error analysis for the physical sciences. McGraw-Hill, New York. (2003).

[79] P. Mali *et al.*, Can. J. Phys. 89, 949 (2011).

[80] I. Derado *et al.*, Z. Phys. C 47, 23 (1990).

[81] G. Alexander and E. K. G. Sarkisyan, Phys. Lett. B 487, 215 (2000); Nucl. Phys. B (Proc. Suppl.) 92, 211 (2001).

[82] M. Adamus *et al.*, (NA22 Collaboration), Phys. Lett. B 185, 200 (1987).

[83] E. K. G. Sarkisyan *et al.*, Phys. Lett. B 347, 439 (1995).

[84] Ph. Brax and R. Peschanski, Nucl. Phys. B 346, 65 (1990).

[85] L. Lianshou, F. Jinghua and W. Yuanfang, Phys. Lett. B 444, 563 (1998).

[86] A. Bershadski, Phys. Rev. C 59, 364 (1999).

[87] W. Ochs, Z. Phys.C 50, 339 (1991).

[88] Ph. Brax and R. Peschanski, Phys. Lett. B 253, 225 (1991).

[89] I. Sarcevic and H. Satz, Phys. Lett. B 233, 251 (1989).

[90] H. Satz, Nucl. Phys. B 326, 613 (1989).

[91] R. C. Hwa and M. T. Nazirov. Phys. Rev. Lett. 69, 741 (1992).

[92] W. Yuanfang and L. Lianshou, Phys. Rev. Lett. 70, 3197 (1993).

[93] L. Lianshou *et al.*, Z. Phys. C 69, 323 (1996).

[94] E. A. De Wolf, In Proceeding of the Ringberg Workshop on Multiparticle Production, Edited by R. C. Hwa *et al.*, World Scientific, Singapore (1992).

[95] P. Carruthers, H. C. Eggers and I. Sarcevic, Phys. Lett. B 254, 258 (1991);
P. Carruthers, H. C. Eggers and I. Sarcevic, Phys. Rev. C 44, 1629 (1991).

[96] N. Suzuki *et al.*, Phys. Rev. C 58, 1720 (1998).

[97] N. Suzuki and S. Suzuki, Prog. Theor. Phys. 62, 727 (1979).

[98] E. K. G. Sarkisyan, Phys. Lett. B 477, 1 (2000);
G. Abbiendi *et al.* (OPAL Collaboration), Phys. Lett. B 523, 35 (2001).

[99] R. C. Hwa, Proc. VII International Workshop on Multiparticle Production, World Scientific, Singapore, p.303 (1997).

[100] L. K. Gelovani, G. L. Gogiberidze and E. K. Sarkisyan, Proc. VIII International Workshop on Multiparticle Production, Matrahaza, Hungary, p.334 (1998).